Student thesis series INES nr 619

The impact of CO_2 fertilisation on foliage in West and East Africa

Gaetane Demyttenaere

2023
Department of
Physical Geography and Ecosystem Science
Lund University
Sölvegatan 12
S-223 62 Lund
Sweden

Gaetane Demyttenaere (2023).
The impact of CO_2 fertilisation on foliage in West and East Africa (English)
Master degree thesis, 30 credits in *Physical Geography and Ecosystem Sciences*
Department of Physical Geography and Ecosystem Science, Lund University

Level: Master of Science (MSc)

Course duration: *January* 2023 until *June* 2023

Disclaimer

The impact of CO_2 fertilisation on foliage in West and East Africa

---

Gaetane Demyttenaere

Master thesis, 30 credits, in *Physical Geography and Ecosystem Science*

Supervisor 1 Torbern Tagesson
Department of Physical Geography and Ecosystem Sciences, Lund University

Exam committee:
Examiner 1, Annemarie Eckes-Shephard
Department of Physical Geography and Ecosystem Sciences, Lund University

Acknowledgements

First of all, I would like to thank my supervisor Torbern Tagesson for all the help he provided throughout the thesis, as well as my friends for all the mental support, brainstorming and study sessions. I would further like to thank the Centre de Suivi Ecologique (Dakar) for collecting and providing the plant biomass data and additionally those working at the Dahra site.

Abstract

Anthropogenic impact on terrestrial ecosystems continues to grow as we further enhance atmospheric Carbon Dioxide (CO_2) concentrations. The changing climatic conditions and direct influence of CO_2 on vegetation has a big impact on ecosystem functions. Such impacts include CO_2 fertilisation, found to be an important driver of the global greening trend. By increasing leaf photosynthesis and enhancing water use efficiency, CO_2 fertilisation stimulates gross primary productivity and increases carbon storage. Isolating this phenomenon from other drivers of plant growth is however difficult. In this thesis I show that CO_2 fertilisation has had a positive influence on semi-arid and arid region in East and West Africa over the period 1982 - 2015. From Earth observations, it was found that the slopes of the relationship between precipitation and maximum fractional foliage, assumed to be a proxy for CO_2 fertilisation, indicated greater production under the same precipitation levels at the end of the study period. It is discussed that this trend will continue in the future unless the response to CO_2 fertilisation reduces, or long-term negative influences on nutrient mineralization occurs. East and West Africa are predicted to become more prone to extensive droughts and higher temperatures under these enhanced CO_2 concentrations, and thus, improving our understanding of the implications of these conditions is becoming ever more important.

Table of Content

1. Introduction

With atmospheric Carbon Dioxide (CO_2) concentrations continuously rising, the impact on the terrestrial ecosystems continues to grow (Bendall et.al., 2022). Both the changing climatic conditions as well as the direct effect of CO_2 on vegetation is affecting ecosystem functions (Dieleman et.al., 2012). Plant growth and photosynthesis increase under enhanced CO_2 (eCO_2) concentration, promoting net primary production and soil carbon (C) storage, but may also increase soil CO_2 emissions back to the atmosphere (Liu et.al., 2018). Understanding the consequences of these new conditions is becoming ever more important to understand the implications of climate change and predicting future changes.

A global greening trend has been identified in over 50 % of the terrestrial surfaces; a trend which can to a large extent be explained by CO_2 fertilisation (Zhu et.al., 2016). This has been found to be apparent within semi-arid regions where precipitation is the dominating limiting factor to plant growth (Fensholt et.al., 2012). However, a study by Boone et.al. (2018), used within the 6th assessment report of the Intergovernmental Panel on Climate Change (IPCC), found a negative plant response to eCO_2 in semi-arid regions of West Africa. They used an ecosystem model, the G-Range model, and simulated the projected effect of eCO_2 under the most aggressive Representative Concentration Pathway (RCP8.5) formulated by the IPCC (Schwalm, Glendon & Duffy, 2020). The modelled eCO_2 effect resulted in a negative trend in above and below ground biomass, herbaceous and annual net primary productivity, and herbaceous cover within West Africa. East Africa on the other hand was shown to be less sensitive to eCO_2 in comparison (IPCC, 2022).

CO_2 is an essential input for photosynthesis (Wong, 2020). As a plant becomes exposed to higher concentrations of CO_2 leaf photosynthesis is stimulated, reducing their stomata opening and increasing water-use efficiency (WUE). These effects lead to stimulated gross primary productivity, increased C storage and overall greater photosynthesis efficiency. This is called CO_2 fertilisation (Holden et.al., 2013; Gifford, 2004). It has however also found that under consistently higher CO_2 concentrations plants may experience decreased stomatal conductance, decreased water use and decreased specific leaf area (Gifford, 2004).

CO_2 fertilisation is a phenomenon that is difficult to observe (Heffernan, 2013) and isolate from the effect of other essential drivers of greening such as light, water and nutrient availability (Donohue et.al., 2013). By focusing on warm, arid environments, where water is the dominant factor constraining primary production, and where foliage cover, water use and photosynthesis are strongly coupled, this complexity can be reduced, highlighting the influence of CO_2 on plant productivity (Donohue et.al., 2013). Under these conditions a curvilinear dependence of foliage on precipitation can be found, with a clear upper edge for maximum foliage highlighting a limit to foliage in a water-limited environment. Changes in this maximum foliage, under stable precipitation conditions, is assumed to be attributed to changes

in CO_2 concentrations, allowing for the analysis of the effect of CO_2 fertilisation (Donohue et.al., 2013).

1.1. Aim

The aim of this thesis is to investigate if the modelled difference in CO_2 fertilisation, seen in the model simulations using RCP8.5 for East and West Africa, can already be confirmed today using satellite-based Earth observations. The relationship between foliage cover from remotely sensed data and precipitation will be quantified. The analysis will also be validated with independent in-situ observations of biomass.

In accordance with the results of the G-Range model, used in the IPCC report, it is hypothesized that Earth observations will show a reduction between 1982-2015 in the response of maximum foliage cover to precipitation (assumed to be a proxy for the CO_2 fertilisation effect) (Donohue et.al., 2013) in West Africa, whereas East Africa will show little or no such response (Boone et.al., 2018; IPCC, 2022). Hence, with this thesis I aim at answering the following research questions:

1. How has foliage cover changed between 1982-2015 in semi-arid regions of East and West Africa?
2. Does CO_2 fertilisation influence trends in foliage cover differently in East and West Africa?

2. Background

2.1. Satellite Remote Sensing of Vegetation

Obtaining information about an object or area using electromagnetic radiation from a distance is known as remote sensing, allowing for the collection of data on multiple environmental processes, the Earth's surface, subsurface and atmosphere (Jong et.al., 2004; Yang et.al., 2013). This process is initiated by the electromagnetic radiation from the sun or from the satellite itself, and from the spectral reflectance, a function of the reflected solar radiation to the wavelength (Karthikeyan et. al., 2020; Jong et.al., 2004). The incident radiation is absorbed, transmitted, or reflected while interacting with the Earth's surface. The reflected radiation contains information about the terrestrial processes taking place. Different processes will reflect radiation at varying wavelengths (Karthikeyan et.al., 2020; Assmann et.al., 2018).

The reflected or emitted radiation is measured using sensors on the satellite (Chuvieco, 2016). These sensors can measure various wavelengths on the electromagnetic spectrum, of which the most common for vegetation are within the visible spectrum (VIS) (0.4-0.7 μm) and the infrared spectrum consisting of near infrared (NIR) (0.7-1.3 μm), mid-infrared (MIR) (1.3-3.0 μm) and thermal infrared (TIR) (3.0-14 μm) (Karthikeyan et. al., 2020). In the case of VIS to MIR the solar radiation reflected by the Earth's surface is measured, whereas for TIR, it is the emitted radiation that is measured. This radiation is however still caused by absorption of the solar irradiance (Jong et.al., 2004).

The spectral properties of vegetation reflect a combination of physical and biochemical canopy attributes, including 'the role of leaf biochemical, plant physiologic, and canopy structural and morphologic properties' (Chuvieco, 2016). These are dependent on light, water, and nutrient availability. Additionally, structural properties such as leaf area index (LAI), fractional vegetation cover, plant height and leaf water need to be considered. Any changes in these aspects will lead to variations in the vegetations' spectral reflectance (Chuvieco, 2016).

The absorbing effect of leaf pigments, in the blue region, and chlorophyll a, chlorophyll b, carotenoids and xanthophylls, in the red region, leads to low reflectance within the VIS region (Chuvieco, 2016). The chlorophyll absorbs red wavelength and the mesophyll leaf structure scatters NIR (Pettorelli et.al., 2005). Between the red and VIS regions lies the lesser absorbed green reflectance peaks, giving the green appearance of healthy vegetation. Beyond this lies the 'red edge', where the leaf pigment and cellulose allow NIR wavelengths to pass through (Chuvieco, 2016). The edge is shifted depending on the plants' nutrient and mineral stress. Once reaching the NIR reflectance plateau (0.70 – 1.1 μm), the reflectance of plants becomes high (Chuvieco, 2016). Overall, the NIR region is sensitive to leaf structural changes (Imran et.al. 2020). Reflectance decreases sharply beyond this plateau towards the short-wave infrared region, a spectral region strongly absorbed by leaf water (Neinavaz et.al., 2021; Chuvieco, 2016).

Before reaching the earth's surface, or the satellite, the radiation will be influenced by the atmosphere. Particles in the atmosphere such as water vapour and aerosols can lead to the scattering or absorption of this radiation, especially within the visible spectrum (Tao et.al., 2012). The way this influences the radiation is dependent on its wavelength, the condition of the atmosphere or the solar zenith angle, 'the angle that the sun makes with a line perpendicular to the surface' (Cronin, 2014). During scattering the radiation interacts with these particles, forming diffused radiation and redistributing them within the atmosphere (Horvath, 1993). This is assumed to occur after the attenuation of atmospheric absorption (Tao et.al., 2012). With atmospheric absorption the radiation is converted to the internal energy of the absorbing molecule, after which it is transferred as heat (Horvath, 1993). The effects of scattering and absorption can reduce the accuracy of the images produced (Fraser & Kuafman, 1985).

2.1.1. NDVI

Vegetation indices can be produced through a combination of bands from multi-spectral remotely sensed images (Huang et.al., 2021). Of these indices, the Normalized Difference Vegetation Index (NDVI) is the most commonly used (Karthikeyan et. al., 2020). NDVI measures the level of greenness of the plant. The photosynthetic pigment in leaves absorb photosynthetically active radiation (Red radiation) (Piao et.al., 2020), and the NIR is scattered by foliage (Beck et.al., 2006). By capturing the contrast between the red and NIR wavelengths in the vegetation the activity and abundance of leaf chlorophyll pigments can be measured (Xiao & Moody, 2005). In doing so it becomes sensitive to the density, condition, and presence of vegetation (Herrmann, Anyamba & Tucker, 2005). NDVI is calculated using the following equation (de Jong et.al., 2012; Huang et.al., 2021):

$$\boldsymbol{NDVI = \frac{(R_{NIR} - R_{RED})}{(R_{NIR} + R_{RED})}} \qquad \textbf{Equation 1}$$

Here the reflectance of red (R_{red}) decreases as the chlorophyll absorption increases and reflectance of NIR (R_{NIR}) increases with increasing green plant biomass. NDVI ranges between -1 and 1, where the former often represents values from clouds, water or snow and the latter dense vegetation and values close to zero represent bare ground (Huang et.al., 2021).

It has been confirmed that NDVI is closely related to several vegetation variables, such as LAI, absorption of photosynthetically active radiation, biomass, chlorophyll concentration, plant productivity, fractional vegetation cover and plant stress (e.g., Olsson, Eklundh & Ardö 2005; Tagesson et.al., 2015; Huang et.al., 2021). These associations allow it to effectively differentiate between different ecosystems and biozones at multiple scales (Pettorelli et.al., 2005). NDVI is well suited in semi-arid areas with sparse vegetation as it becomes saturated at high LAI levels. Furthermore, semi-arid regions are less prone to cloud issues, as would be the case for forested tropical regions, making the results more reliable (Olsson et.al., 2005).

2.2. Arid and Semi-Arid Ecosystems

Arid and semi-arid ecosystems cover over a third of global land area (Nielsen & Ball, 2015) and provide important ecosystem services such as food, grazing and energy (Fensholt et.al., 2012). Here plant growth is mostly limited by water availability (Hickler et.al., 2005; Helldén & Tottrup, 2008), and evapotranspiration generally exceeds precipitation. However, factors such as incoming shortwave radiation, temperature and nutrients can also influence growth (Fensholt et.al., 2012).

2.2.1. Greening Trend

There has been a noticeable greening trend (Fensholt et.al., 2012; Helldén & Tottrup, 2008; de Jong et.al., 2012), including in semi-arid areas such as the Sahel (Hickler et.al., 2005; Olsson et.al., 2005; Herrmann et.al., 2005; Anyamba & Tucker, 2005). This is represented by a global increase in NDVI of 0.015 NDVI units between 1981 and 2007 (Fensholt et.al., 2012) and an increase of up to 59 % from the 1980s (Piao et.al., 2020). This increased greenness can for example be represented by an increase in average leaf size, plant density or leaf number per plant. Vegetation models suggest that this trend, at a global scale, is driven by CO_2 fertilisation (Piao et.la., 2020; Fensholt et.al., 2005).

Within semi-arid regions a high correlation has been found between NDVI and rainfall (Herrmann et.al., 2005; Fayech & Tarhouni, 2021). An increase of up to 50 % in average NDVI in parts of West and East Africa was found when comparing 2002-2007 to 1982-1987 (Herrmann et.al., 2005), as both NDVI and rainfall increased, especially during the wet season and after the great Sahelian drought (Fensholt et.al., 2012; Herrmann et.al., 2005; Anyamba & Tucker, 2005; Helldén & Tottrup, 2008; Piao et.al., 2020; Zhu et.al., 2016). The conditions during the wet season increased maximum NDVI, whereas the length of the growing season remained constant. More specifically, the increased greenness was related to soil moisture which is a function of rainfall over time (Ahmed et.al., 2017; Hermann et.al., 2005). However, Olsson et.al. (2005) found that only half of the rainfall stations that showed an increase in NDVI also showed rising precipitation. Furthermore, only 8 out of 40 of their rainfall observations showed a statistically significant increase in precipitation between 1982-1990 and 1991-1999, leading them to conclude that only part of the increase in vegetation can be explained by rising precipitation. This was further confirmed by Herrmann et.al. (2005), who interpreted the increase in rainfall as a return to normal conditions after the drought period from the late 1960s to early 1980s.

When the changes in NDVI, within semi-arid regions, have been normalised for rainfall, trends are not completely removed (Hermann et.al., 2005). In other words, the greening trend can also be attributed to other climatic factors such as rising CO_2 concentrations, increased temperatures and enhanced growing season length, and not solely by rainfall trends

(Helldén & Tottrup, 2008). Human-induced changes in vegetation have additionally been found through rural-to-urban migration (increasing agricultural abandonment) and fuel-wood collection causing a browning trend and increased investment in land management, land use change from agricultural intensification or extensification, introduction of large-scale irrigated agriculture and afforestation causing a greening trend (Hickler et.al., 2005; Olsson et.al., 2005; Piao et.al., 2020). Despite this there has been little effort made within studies to separate human-induced changes from the climatic ones (Herrmann et.al., 2005).

In East Africa it was found that more than 60 % of the land experienced a greening trend before the 1990s, but this trend has stalled, or reversed to a browning trend, for over 50 % of the land area, between 1982 and 2013 (Wei et.al., 2018). The area was found to have a stronger correlation with soil moisture than with precipitation, likely due to the lag effects of precipitation on vegetation growth (Wei et.al., 2018). A possible explanation would be the turn to a more growth-hostile climate at the start of the 21st century. There was a shift from a cooling and wetting trend towards a warming and drying one, decreasing plant water availability for growth and increasing water deficits (Wei et.al., 2018).

2.2.2. Climate in West and East Africa

Many regions in Africa are experiencing more extreme changes in the climate in comparison to the global average (Ranasinghe et.al., 2021). With the exception of northern and southwest Africa, the entire continent is expected to experience rising mean temperatures and an increase in frequency and intensity of heavy precipitation. This is evident in West Africa, where temperatures have risen by 1-3 °C since the mid-1970s and are projected to rise by 2 °C and 5 °C by the end of the century under mid and high emission scenarios respectively (e.g., Nikiema et.al., 2017; Ranasinghe et.al., 2021). Furthermore, the combination of anthropogenic aerosol and greenhouse gas emissions, that had caused a decline in rainfall between the 1950s and 1980s, shifted in the 1990s to intense, but infrequent precipitation events (e.g., Giannini & Kaplan, 2019; Booth et.al., 2012; Kennedy et.al., 2017). Under mid and high emission scenarios this trend is expected to continue, along with an overall more drought prone, arid climate (e.g., Sylla et.al., 2016; Dosio et.al., 2021).

In East Africa the temperatures have risen by 0.7 - 1.0°C since the mid-1970s, and temperatures will increase further under both mid and high emission scenarios (Ayugi & Tan, 2019; Camberlin, 2018). Precipitation has showed varying trends, with the equatorial regions experiencing a wetting trend within the short rains (October - December) (Manatsa & Behera, 2013; Nicholson, 2017), but a drying trend and shortening of the longer wet season (March – May) (Rowell et.al. 2015; Wainwright et.al., 2019). Thus, different trends are found at different seasons of the year. Since 2000 a strong relationship can be found with droughts occurring during La Niña events, and wetter periods with a strong Madden-Julian Oscillation (Park et.al., 2020; Funk et.al., 2018). It is projected that the short rainy season will be elongated, with higher rainfall and with an increase in heavy rainfall events (Gudoshava et.al., 2020). Despite this,

drought frequency, duration and intensity are expected to increase in the northern regions (e.g., Liu et.al., 2018; Nguvava et.al., 2019).

2.3. Carbon Dioxide

2.3.1. Rising CO_2 Concentrations

Humans have contributed to climate change through the release of CO_2 into the atmosphere (Ekwurzel et.al., 2017). Data from NOAA (2022) shows how atmospheric CO_2 concentrations have grown from 336 μmol mol^{-1} CO_2 in 1979 to 416 μmol mol^{-1} CO_2 in 2022. With ever growing emissions ecosystems and their vegetation continue to be affected by the changing conditions. These include the direct influence of rising atmospheric CO_2 concentrations, as well as the influence of rising temperatures and varying precipitation levels (IPCC, 2022).

2.3.2. CO_2 Fertilisation

Changes in long-term vegetation greenness is driven by land-use changes and biogeochemical effects, including regional climate change, nitrogen deposition and the fertilisation effect of eCO_2 concentrations (Zhu et.al., 2016; Smith et.al., 2020). One of the primary substrates of photosynthesis is CO_2, thus, increasing its availability is expected to lead to a fertilisation effect with enhanced photosynthesis (Donohue et.al., 2013). Through the process of photosynthesis, atmospheric CO_2, water and sunlight are used to synthesize carbohydrates (Boretti & Florentine, 2019). Light is absorbed by the pigment-protein antenna complexes and efficiently converted into redox chemical energy (Stirbet et.al., 2020), driving the primary photosynthetic energy conversion process (Krause & Weis, 1991). Water is oxidized and the CO_2 is assimilated in the stroma within the Calvin-Benson cycle, where the CO_2 is reduced to energy-rich carbohydrates (Shevela & Bjorn, 2018).

The physiological processes of transpiration and photosynthesis can be directly affected by eCO_2 concentrations (Wiltshire et.al., 2013). The magnitude of this physiological forcing is dependent on the plants' stomatal control over evapotranspiration. This response is species dependent, with two main pathways in which the plant fixes CO_2 during photosynthesis, namely, C3 and C4, depending on the environmental conditions in which the plant survives. While C3 plants prefer cooler conditions, between 18-24 °C, C4 plants prefer warmer temperatures, between 32- 55 °C (Boretti & Florentine, 2019). Additionally, C3 and C4 species prefer either wet or dry environments respectively (Boretti & Florentine, 2019). Sonmez et.al., (2022) found that under current CO_2 concentrations C4 plants have been found to be more efficient than C3 plants, but their response to eCO_2 concentrations is still uncertain. Ghannoum et.al., (2000) found that the growth stimulation of C4 plants in response to a doubling in CO_2 concentration was lower than that of C3 plants, with changes of 22 - 33 % and 40 - 44 % respectively.

It was found that evapotranspiration was reduced within environments with eCO_2 concentrations, and in turn possibly increasing the plants' WUE (Wiltshire et.al., 2013; Zhang et.al., 2022). WUE can be defined as 'C uptake per unit water loss through transpiration' (Smith et.al., 2020). The degree of stomatal opening, and thus conductance, is reduced under elevated CO_2 concentrations, therefore limiting the potential water loss through evapotranspiration. Simultaneously the uptake of CO_2 remains approximately the same as the higher concentrations create a larger gradient difference in CO_2 concentrations between the leaf and the surroundings, allowing more CO_2 to be diffused with a smaller stomatal opening (Ghannoum et.al., 2000). This stimulates leaf CO_2 assimilation and growth rates by increasing leaf temperature, conserving soil water, and improving shoot water relations (Ghannoum et.al., 2000). Zhang et.al., (2020) however found that the reduction in canopy stomatal conductance, induced by rising CO_2, could have greatly offset the greening-induced increase in evapotranspiration and canopy transpiration over Eurasia since the 1980s. Additionally, CO_2 fertilisation was found to have a positive influence on light use efficiency, defined as 'the amount of vegetation production per unit radiation absorbed' (Smith et.al., 2020). This can be approximated by measuring changes in gross primary production and fractional absorbed photosynthetic active radiation (Smith et.al., 2020).

2.3.2.1. G-Range Model Predictions

Table 1 Selected results from Boone et.al., (2018) on the influence of CO_2 fertilisation on vegetation in rangelands.

	Above ground live biomass (~ % change)	Herbaceous net primary productivity (~ % change)	Bare ground (~ % change)
West Africa	- 50	- 40	- 5
East Africa	7.5	- 5	7.5

An increased greenness within the Sahel can in part be attributed to CO_2 fertilisation (Helldén & Tottrup, 2008). The results of Boone et.al., (2018) (Table 1) within the 2022 IPCC report however predicts a different trend by 2050. Here plant responses to eCO_2 fertilisation in rangelands were modelled using the G-Range model, showing a sharp decrease, approximately 50 %, in above ground biomass and annual net primary productivity (NPP) in West Africa by 2050 under RCP8.5. East Africa on the other hand showed only slight changes, approximately 7.5 %, with a predicted increase in above ground biomass, and decrease in annual net primary productivity.

The G-Range model was applied at a 0.5 ° x 0.5 ° resolution with spatial data describing deciduous and evergreen trees, shrubs, herbaceous plants and soil properties and cover (Boone et.al., 2018). In the model the plants compete for space, light, water, and nutrients. Additionally, it contains parameters to describe nutrient cycling, fire, fertilization and plant establishment, growth, and death. Parameters to describe 15 biomes were incorporated,

including those for savanna, grassland, or steppe, and open and dense shrubland. Finally, a two-thousand-year long spin-up simulation was run using dynamic monthly precipitation and temperature data from 1901 – 2006.

In modelling the future for 2050, the plants' productivity response with and without eCO_2 fertilisation was analysed. Overall, it was found that increased CO_2 had a greater, and positive, influence on the ecosystem C stock than rising temperatures in rangelands globally. Despite this, a decrease in NPP $\geq$ 250 g C m^{-2} $year^{-1}$ in the semi-arid savannas south of the Sahara was found in West Africa (Boone et.al., 2018).

2.3.2.2. Remote Sensing of CO_2 Fertilisation in Arid Ecosystems

By focusing on arid and warm environments where water is the limiting factor to plant growth, photosynthesis and foliage cover, the effect of CO_2 fertilisation can be isolated (Donohue et.al., 2013). In these regions where moisture is the main limitation on plant growth, the effect of CO_2 on vegetation in expected to manifest most strongly (Ukkola et.al., 2016). Foliage was found to have a curvilinear relationship to precipitation, with a near linear relationship under arid conditions (Donohue et.al., 2013). With low precipitation, between 0 - 400 mm of rain per year, an upper edge can be identified as the maximum foliage under certain precipitation levels. The linearity of this relationship shows the constraint to foliage for environments where water is the limit to growth (Donohue et.al., 2013). It was found that this upper edge was independent to vegetation and climate types. It was thus hypothesized that CO_2 concentrations play a role in setting this upper limit, as it plays an important role in transpiration and photosynthetic rates, with increasing CO_2 concentration increasing the upper edge (Donohue et.al., 2013).

3. Methodology

3.1. Study Area

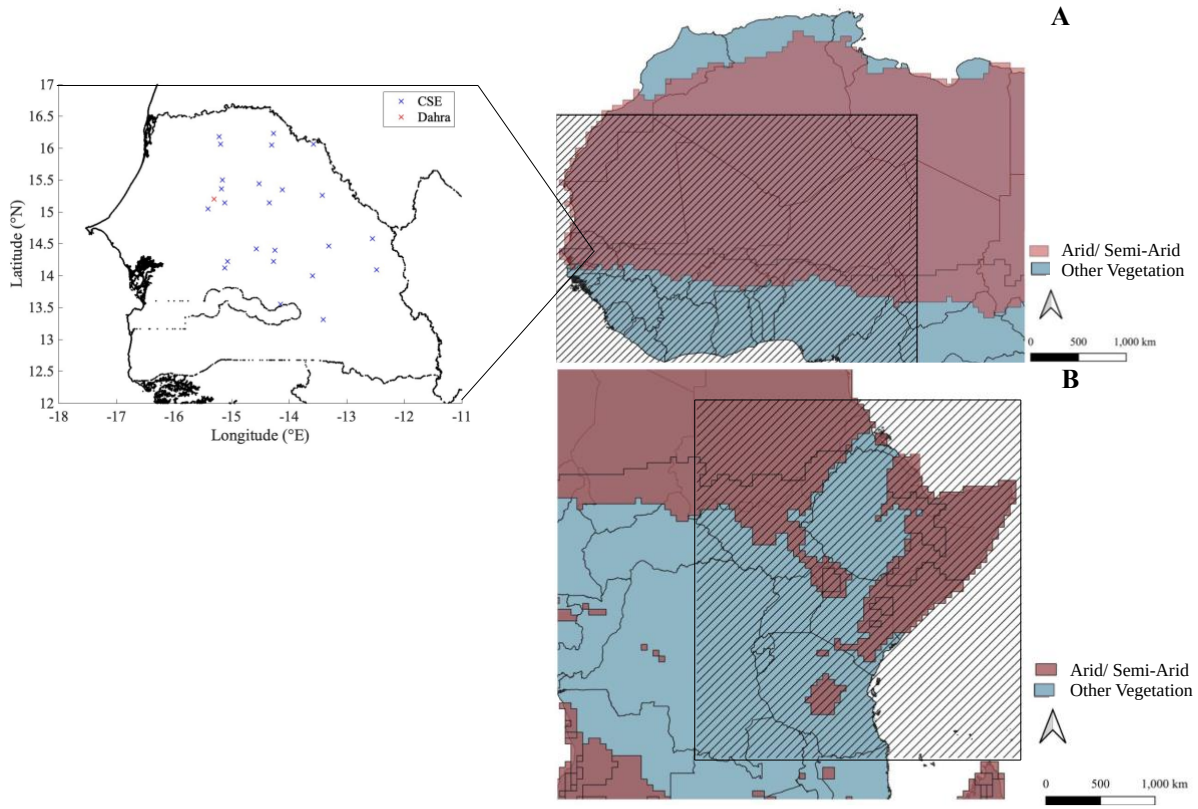

Figure 1 Area selection of semi-arid and arid land areas in West Africa (A) and East Africa (B) (openAfrica, 2020) according to the Köppen-Geiger classification system (Worldbank, 2023). Here the red area represents those areas classified as arid or semi-arid and the black lined box the area for which data was collected for West Africa. The field observation points in Senegal are pointed as blue x's (CSE site) and the red x (Dahra site).

Within this thesis, arid and semi-arid regions in West and East Africa were studied (Figure 1). West Africa shows a strong north-south gradient in climate, but also in vegetation cover (Knauer et.al., 2014). The Sahara is found in the north, a region with extremely sparse vegetation. More south the Sahel can be found, this region has a sparse tree and shrub layer with sparse to closed grasslands. This region is strongly water-limited, meaning the growing season is mostly confined to the rainy season. Within the Sahel a rainfall gradient is present, moving from 150 – 300 mm annual rainfall in the northern regions, to 500 – 700 mm in the southern regions (Tian et.al., 2016). Within this region the Dahra and Centre Suvi Ecologique (CSE) study sites can be found, both located in Senegal, and these provide field observations for evaluation of the Earth observations. The Dahra site can be described as a shrub and low tree savannah with continuous, but seasonal grass cover with a light tree cover (Tagesson et.al., 2015). The CSE site can be described as a savannah containing shrubs and woody and

herbaceous trees (Tian et.al., 2016). Further south in West Africa the environment is no longer water limited (Knauer et.al., 2014).

East Africa is predominantly semi-arid, making it a rainfed environment (Kalisa et.al., 2019). It can be divided into six main vegetation communities, namely, 'mangrove, coastal rainforest, open savannah grasslands, wooded savannah, montane forest, and Ericaceous shrub' (Marchant et.al., 2018). The grasslands dominate the region, with agriculture and woodlands being spread throughout, and patches of bare soil found in the north (Kalisa et.al., 2019).

3.2. Data Collection and Pre-Processing

3.2.1. Gridded Data

Multiple data sets were used in this analysis (Table 2). Firstly, the Global Inventory Modelling and Mapping Studies (GIMMS) NDVI, which is the most commonly used data set with global coverage of NDVI from as early as 1981 (Fensholt et.al., 2012). With its 1/12 ° by 1/12 ° spatial resolution it is considered the best dataset for long term NDVI studies and was found to have a high correlation with the higher resolution MODIS dataset in semi-arid regions (Fensholt et.al., 2012; Pettorelli et.al., 2005; Tian et.al., 2015). Additionally, GIMMS NDVI has been corrected for aerosols present in the atmosphere, making it ready for analysis (de Jong et.al., 2012).

ERA5-Land is a 0.1° by 0.1° resolution reanalysis dataset on the evolution of land variables. It creates a global set of model data with observations over several decades, starting in 1950 (Copernicus, 2022). Monthly precipitation data from 1982 – 2015 from ERA-5 Land was used within this analysis.

Finally, the Köppen-Geiger land classification data set was used to identify the arid and semi-arid regions. The studied areas were selected according to the Köppen-Geiger land classification using long term monthly precipitation and temperature data to aggregate climate gradients (Peel et.al., 2007; Beck et.al., 2018). In the classification process the classes were firstly divided into five main vegetation groups: equatorial (A), arid (B), warm temperate (C), snow (D) and polar (E), followed by the classification of precipitation and temperature respectively (Kottek et.al., 2006). From the Köppen-Geiger climate classification, areas describing arid environments, classified as 'B', in both West and East Africa were selected as study area (figure 1).

Table 2 Data sources with specification for the Normalized Difference Vegetation Index (NDVI) from the Global Inventory Modelling and Mapping Studies (GIMMS) dataset, precipitation from the ERA5-Land dataset, land classification from the Köppen-Geiger classification and biomass from the Dahra and Centre Suvi Ecologique (CSE) sites.

Data	Available Timespan	Frequency	Source/ Site
NDVI	1982- 2015	Semi-monthly	GIMMS
Precipitation	1950- 2022	Monthly	ERA5-Land (Copernicus, 2022)
Land Classification	-	-	Köppen-Geiger (World Bank, 2023)
Biomass	2006-2022	Semi-monthly (June-October)	Dahra, Senegal (Tagesson et.al., 2015)
	1987-2022	Yearly (October)	CSE sites, Senegal (Diouf et.al., 2015)

3.2.1.1. Pre-Processing

The precipitation data was collected for every individual year from ERA5-Land and handled according to the webpage of Copernicus (2022). This meant adjusting the data for their individual offset and scale factor and converting from daily to monthly values (Copernicus, 2022). The precipitation data within the arid areas, identified within figure 1, were selected. This was further filtered by selecting only those longitude and latitude combinations present in both the precipitation and NDVI datasets. This was necessary seeing as the two data sets initially had different resolutions, causing not all combinations to be present in both datasets. Next, the data of three consecutive years was selected using a moving window. This resulted in grouped data for the years 1982 – 1984, 1983 – 1985 … 2013 - 2015. This was done to limit the year-to-year transient effect. In doing so the conditions and results of the previous and following year were also considered.

The semi-monthly NDVI data and their corresponding flags were collected from GIMMS. These flags represent the quality of the data set and range from 1 - 3 representing high to low quality data respectively. Those datasets flagged with 3 were replaced with 'NaN' as they were identified as low quality. To make the NDVI data comparable to precipitation, the resolution was resampled from 1/12 ° x 1/12 ° to 1/10 ° x 1/10 ° using 'nearest neighbour'. Furthermore, the semi-monthly values were transformed to monthly values by selecting the maximum value per cell, per month. This was done to find the highest NDVI values under the precipitation conditions as NDVI is generally decreased due to errors such as cloudiness and aerosols (Vickers et.al., 2016). Again, the data for three consecutive years was combined using a moving window.

3.2.2. Field Observation Evaluation Data

Biomass data was collected from two sources in Senegal, namely the Dahra and the CSE sites. These include green vegetation, dry matter, and water content data for the Dahra site (Tagesson et.al., 2015), and herbaceous biomass, woody biomass, and total biomass from 24 sites across Senegal collected by CSE (Diouf et.al., 2015). Of these the dry matter and total biomass were used for analysis for the Dahra and CSE sites respectively.

3.3. Data Analysis

3.3.1. Remote Sensing

3.3.1.1. Precipitation

Following Donohue et.al., (2013), precipitation bins were created up until 400 mm of precipitation. The monthly precipitation was used here rather than annual; thus, a different interval and number of bins was used. 54 precipitation bins were created with an interval of 7.5 mm, up until 400 mm of precipitation. In doing so the data was classified by numbers ranging from 1, for 0 – 7.5 mm precipitation, to 54, for ≥ 397.5 mm precipitation. Within this range (0 - 400 mm of precipitation) the relationship under low precipitation levels was highlighted. With the data sets reaching a maximum of 1843 mm and 617 mm for East and West Africa respectively, the limit of 400 mm was used to be representative of low precipitation. These classification values were later used to bin the fractional foliage values, thus collecting all foliage values present in these precipitation bins.

3.3.1.2. Fractional Foliage

The monthly NDVI values were then transformed to fractional foliage using the following equation (Donohue et.al., 2013):

$$\boldsymbol{F} = \frac{(\boldsymbol{V}-\boldsymbol{V_n})}{(\boldsymbol{V_x}-\boldsymbol{V_n})} \qquad \text{Equation 2}$$

Here V was the selected NDVI value, and V_n and V_x the NDVI value representing no foliage and full green foliage cover respectively. In accordance with Donohue et.al., (2013) V_n was set to an NDVI of 0.15, and all measured values below this were set to 0.15 to represent bare ground. V_x was set to 0.99 as this was the highest NDVI value found within both the data sets for semi-arid and arid vegetation in West and East Africa.

From these foliage values the average maximum per year was extracted and plotted on a timeseries. This showed the general trend in foliage over the study period in both arid and semi-arid study areas in West and East Africa. Furthermore, the average foliage over the entire study period was extracted and plotted on a map for the studied regions. This showed the spatial pattern of vegetation in these areas. Additionally, the trend in foliage between 1982 and 2015 was mapped to locate those areas which experienced the greatest change over the study period.

This was done by finding the linear regression over time from the yearly averages of every pixel. From this the rate of change in every pixel was quantified and then mapped.

3.3.1.3. Relationship Precipitation and Fractional Foliage

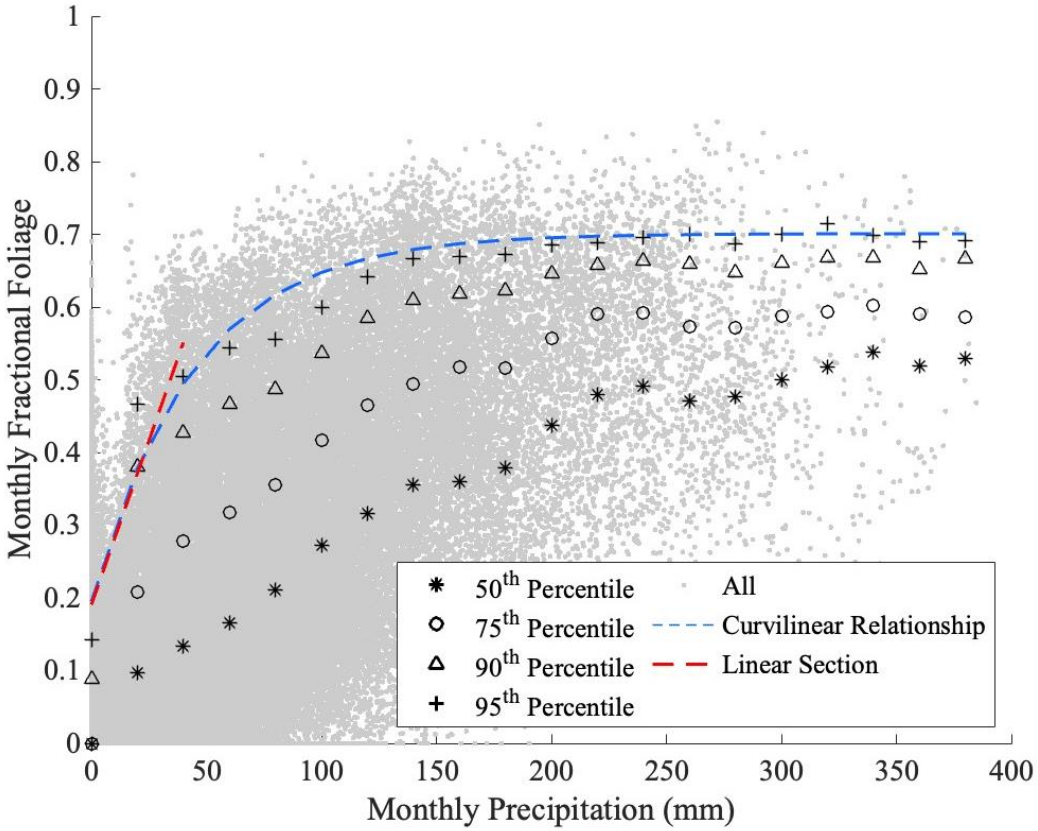

Figure 2 Curvilinear relationship of fractional foliage to monthly precipitation. Here the grey points represent all data point from 1987 in West Africa and the black *, o, Δ, and + are the 50th, 75th, 90th and 95th percentile values for each precipitation bin respectively. The red line represents the linear section on the curvilinear relationship and the blue curve shows the entire curvilinear relationship.

Based on the classification bins of precipitation the fractional foliage values were regrouped for the 3-year moving windows. This resulted in 54 groups of fractional foliage per 3 years. Within these bins the 95th percentile values of fractional foliage were extracted and then used for further analysis. The 95th percentile values were chosen as they best represented the upper edge of the curvilinear relationship between precipitation and fractional foliage, while still avoiding issues with outliers (figure 2) (Donohue et.al., 2013).

The 95th percentile fractional foliage values were plotted against their corresponding precipitation level bins. Following Donohue et.al., (2013), a linear relationship was fitted using ordinary least squares regression between the precipitation level bins and the 95th percentile fractional foliage values ranging from 0.05 to 0.55. In doing so solely the linear section of the curvilinear relationship was selected, resulting in a relationship similar to the red dashed curve in figure 2 for every year.

Secondly, a curvilinear relationship was fitted between all 95th percentile fractional foliage values and their respective precipitation bins with the following equation:

$$\boldsymbol{y = (a + c) \times (1 - e\left(\frac{-bx}{(a+c)}\right) + c} \qquad \textbf{Equation 3}$$

Here *y* is the 95th percentile fractional foliage, and *x* the precipitation bin value, *a* is the point at which the curve transforms from a linear to a curved relationship, *b* is the slope at the intercept (representing NDVI increase per rainfall), and *c* is the intercept. This resulted in a relationship similar to the blue dashed curve in figure 2 for every year. From both methods the slope of the linear curve, or section, was selected for each year. Additionally, the asymptote of the curvilinear relationship was extracted from *a + c* from every year from the curvilinear relationship.

To identify outliers, the Studentized residuals of each curve were calculated (Ni, et.al., 2018). This method measured how many standard deviations the value differed from the averaged linear regression of the entire study period. The plots ranging 2 standard deviations from the linear regression were identified as outliers, and then removed from further analysis.

The changes in the slopes of the linear curves then represented the changing maximum fractional foliage independent of precipitation, presumably caused by CO_2 fertilisation (Donohue et.al., 2013). By using and comparing the two techniques there would be greater confidence in the results of the slope changes. Time series of the slopes from both methods were plotted to see the changes over time. The standard errors of the trends were calculated, and the Kendall-Tau test was used to test for statistical significance.

Furthermore, the asymptote of the curvilinear relationship was plotted on a time series. This asymptote represents the point at which the vegetation is no longer water limited (Ukkola et.al., 2016), plotting this on a time-series can give further understanding to the response of the vegetation. Again, the overall relationship of the slopes was quantified to estimate trends between 1982 – 2015, and the standard error and the statistical significance, using the Kendall-Tau test, were calculated.

3.3.2. Field Observed Biomass

The Earth Observation based fractional vegetation cover was validated against field observations of biomass. Depending on the study site varying biomass data was used. For the Dahra sites this was dry matter between 2006 and 2021, and for the CSE sites this was total biomass between 1987 and 2022. The CSE data set missed data from the year 2004, and the Dahra data set missed data for the years 2007 and 2020.

The maximum biomass or dry matter per year was extracted for each field observed data set and plotted on a time series to see the general trend in vegetation in the areas. To compare the interannual variability of the field observations with those of the remotely sensed

data, the z-score of the dry matter at the Dahra site and the total biomass at the CSE site were calculated and plotted against the z-score of the NDVI of the pixels in those regions. The z-scores were calculated using the following equation:

$$z = \frac{x-\mu}{\sigma} \qquad \textbf{Equation 4}$$

Here *x* is the raw data value, is the mean of the of the population and σ the standard deviation of the population. This was done to account for the uncertainty in the relationship between field observation and NDVI resulting from factors such as soil effects, grazing pressure, or land use (Dardel et.al., 2015). These z-scores then suggested if the field observed data was comparable to that of the remotely sensed data.

4. Results

4.1. Change in Foliage Cover 1982 - 2015

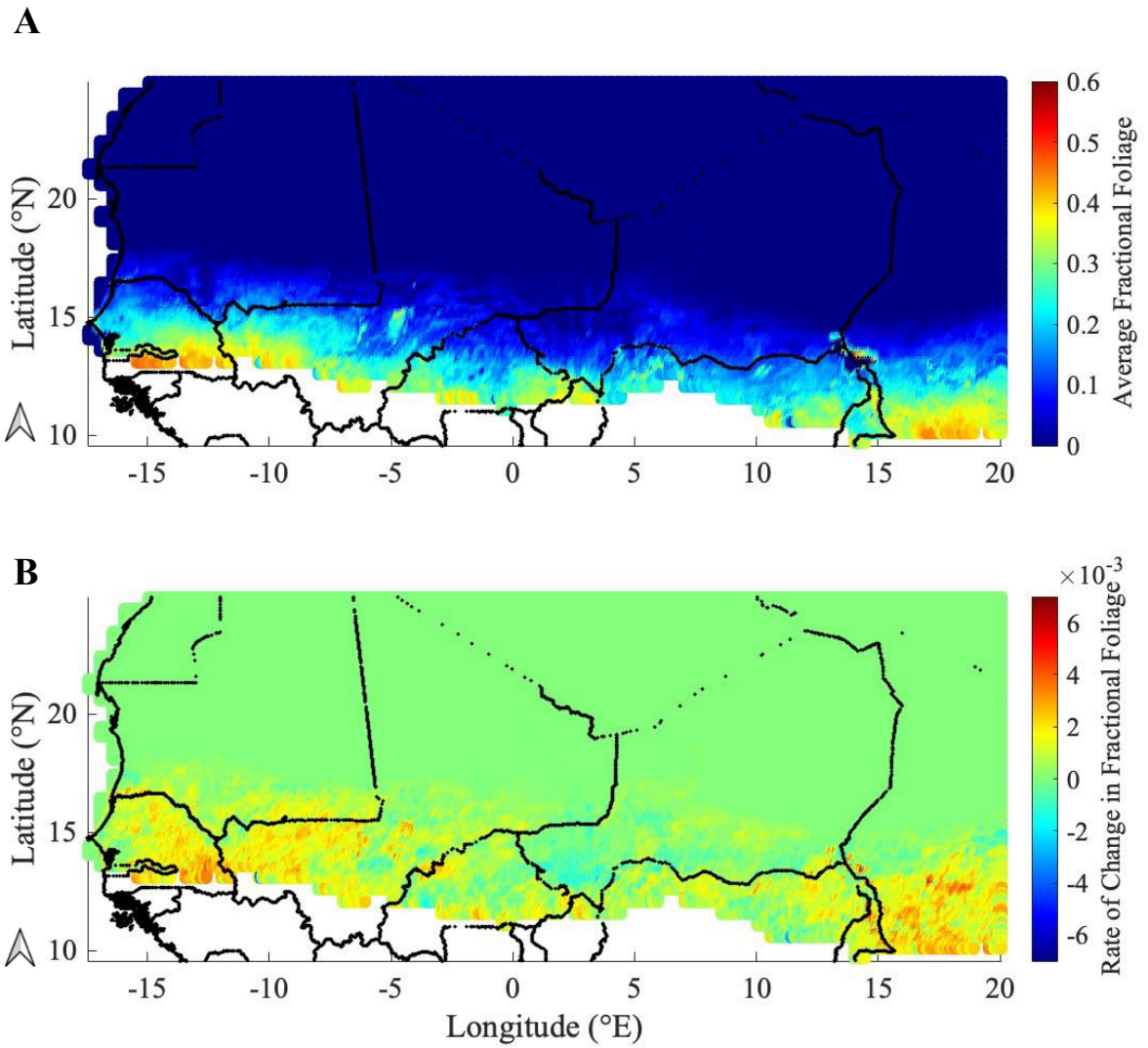

Figure 3 Maps of (A) average fractional foliage during the entire study period (1982 - 2015) and (B) the rate of change in fractional foliage between 1982 and 2015 in the semi-arid and arid regions of West Africa.

A latitudinal gradient in average fractional foliage was seen in West Africa (Figure 3A). Here it was evident that the highest fractional foliage was found in the south of the study area, where fractional foliage values > 0.5 were located. Moving northwards the fractional foliage decreased, finally reaching 0 fractional foliage between 16 and 18 °N.

The largest trends in fractional foliage between 1982 and 2015 in West Africa were found in the southern regions of the study area, specifically between 10 and 18 °N (Figure 3B). Small regions between 15 and 20 °E or between - 10 and 0 °E showed changes with the greatest positive change, with a rate of change > 6 $x10^{-3}$. Patches of decreasing fractional foliage were found between 0 and 5 °E. Above 18 °N no changes in fractional foliage was seen.

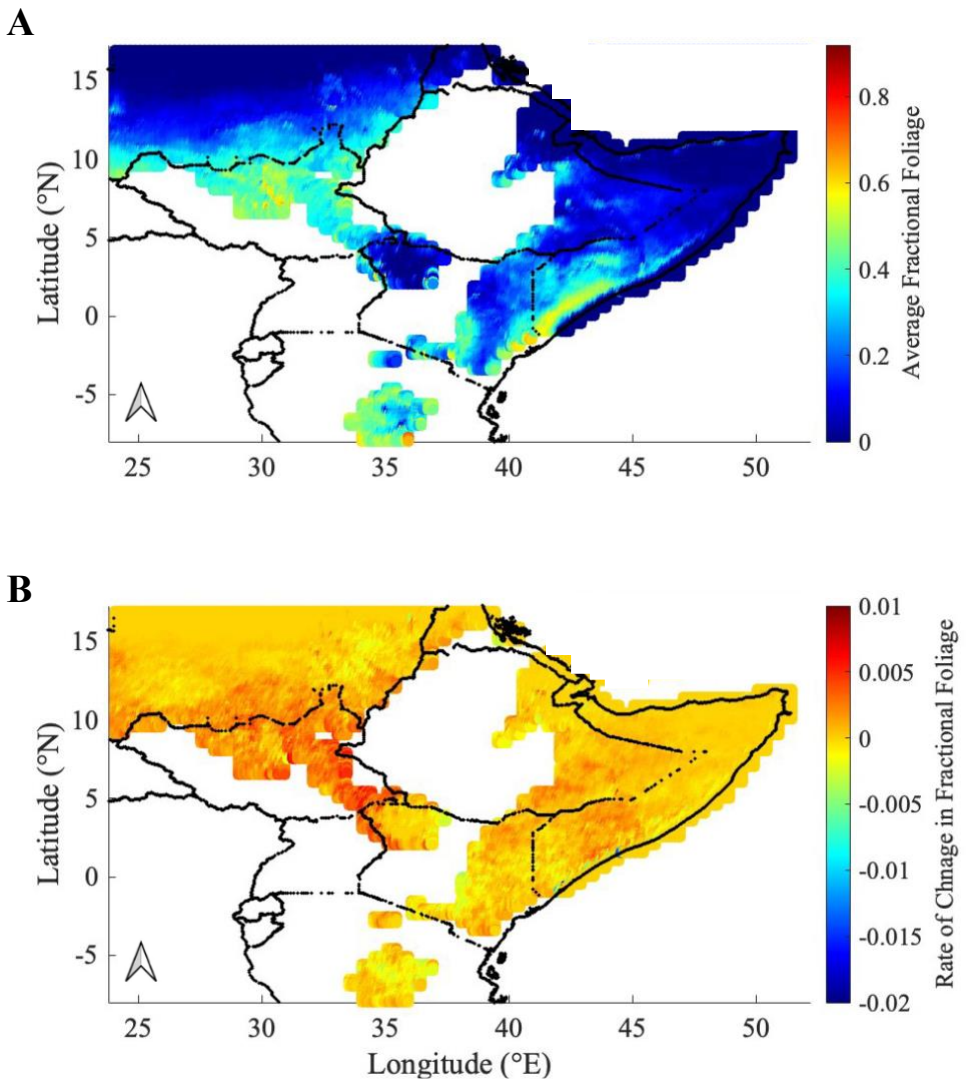

Figure 4 Maps of (A) average fractional foliage during the entire study period (1982 - 2015) and (B) the rate of change in fractional foliage between 1982 and 2015 in the semi-arid and arid regions of East Africa.

There were regional differences in average fractional foliage across the semi-arid and arid regions in East Africa that ranged from 0 to ~ 0.8 average fractional units (Figure 4A). The lowest average fractional foliage was found in the north of the study area, around 15 °N, as well as along the East Coast. Here average fractional foliage was zero. Below this, and moving land inwards to the West, the average fractional foliage increased with large regions ranging between 0.2 and 0.6 average fractional foliage units.

The greatest positive trends in fractional foliage between 1982 and 2015 were located between 3 and 12 °N and 27 and 36 °E, with patches of positive change also found between 40 and 45 °E (figure 4B). Here the rate of change in fractional foliage reaches > 0.005. The negative changes were more spread out, with a patch around 35 °E and 40 °E as well as a horizontal region around 12 °N.

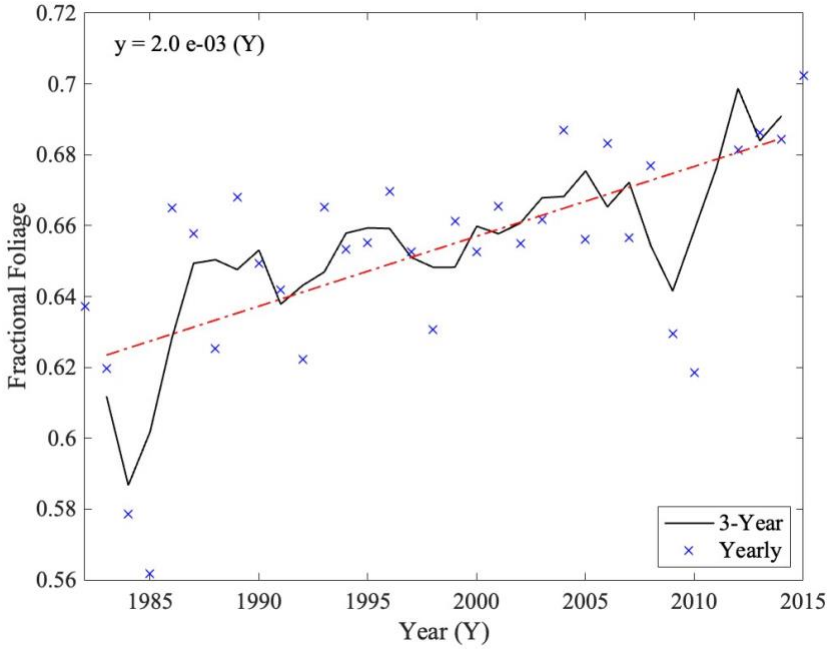

Figure 5 Change in average maximum fractional foliage per year in West Africa. The plotted black line shows the results from the 3-year moving window, the blue x's show the yearly average maxima and the red curve the overall trend over time, as described by y.

There was a positive trend in maximum foliage cover between 1982 and 2015, increasing fractional foliage cover by 2.0 x 10^{-3} per year in West Africa (Figure 5). Within this overall increasing trend some stronger dips in fractional foliage were found, namely in 1984, 1991, 1997, and 2009. These dips were often followed by a strong rise in fractional foliage within the subsequent years. This was seen between 2009 and 2012 where the fractional foliage increased from ~ 0.64 to ~ 0.70 within a year.

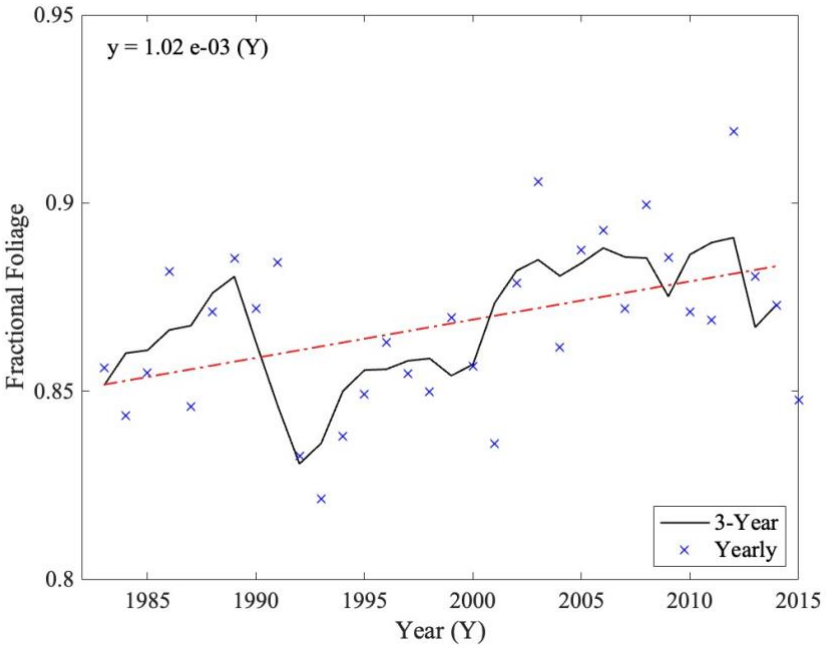

Figure 6 Change in average maximum fractional foliage per year in East Africa. The plotted black line shows the results from the 3-year moving window, the blue x's show the yearly average maxima and the red curve the overall trend over time, as described by y.

There was a rise in average maximum fraction foliage of 1.02×10^{-3} per year between 1982 and 2015 in East Africa (Figure 6). With this overall increasing trend a few years showed dips in fractional foliage, namely around 1992, 2009, and 2013. These dips were often followed by stronger rises in the subsequent years, leading to the overall rising trend. Of these rises the greatest was from 2000 to 2001, where there was a difference of ~ 0.025 fractional foliage units in one year.

4.1.1. Field Observed Biomass

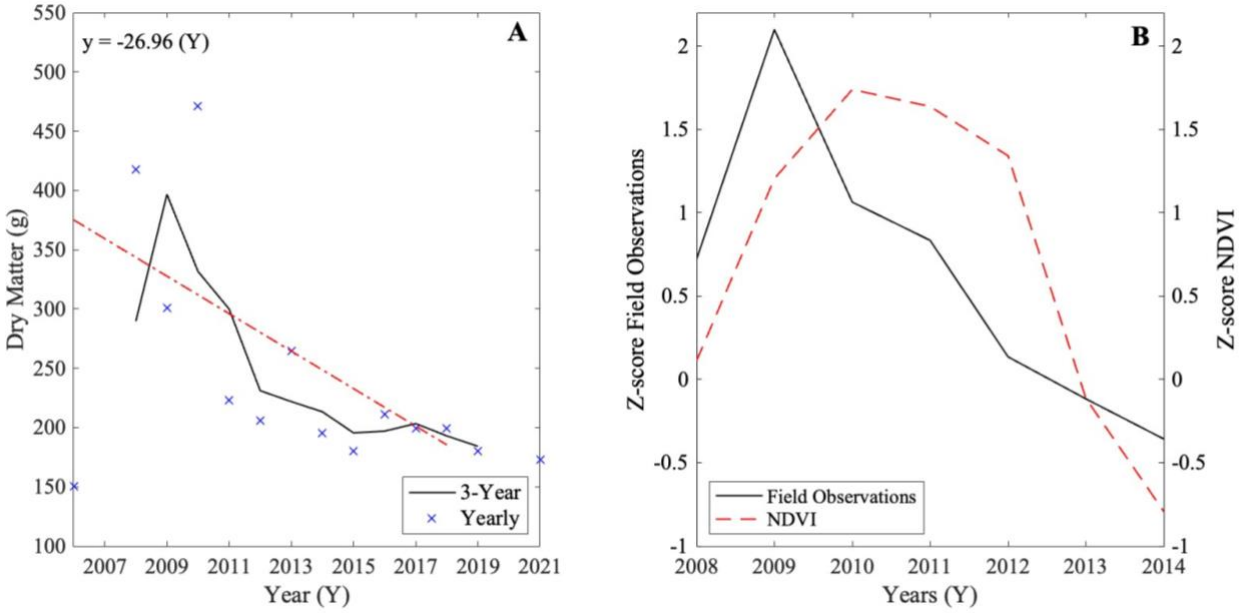

Figure 7 The (A) changes in average maximum dry matter from the field observed data at the Dahra site and the (B) z-score of the field observations and its corresponding NDVI values. In A the black line represents the 3-year moving window, the blue x's show the yearly average maxima and the red curve the overall trend over time described by y. In B the black line shows the field observations and the red dashed line the NDVI.

The Dahra site showed an overall decreasing trend in dry matter of 26.96 g year^{-1} between 2006 and 2021 (Figure 7A). This trend can greatly be explained by the strong decrease in dry matter found between 2009 and 2012 where it dropped from 400 g to ~230 g. After this the dry matter remained more stable moving towards 200 g of dry matter in the following years, with a more gradual decreasing trend.

The z-scores of the field observations from the Dahra site and NDVI showed a similar trend throughout the study period (Figure 7B). The z-scores of the field observations start to decrease from 2009 onwards, whereas those of the NDVI decrease a year later. Both the field observations and NDVI show a positive z-score until 2013, after which it falls below zero and becomes negative. V.

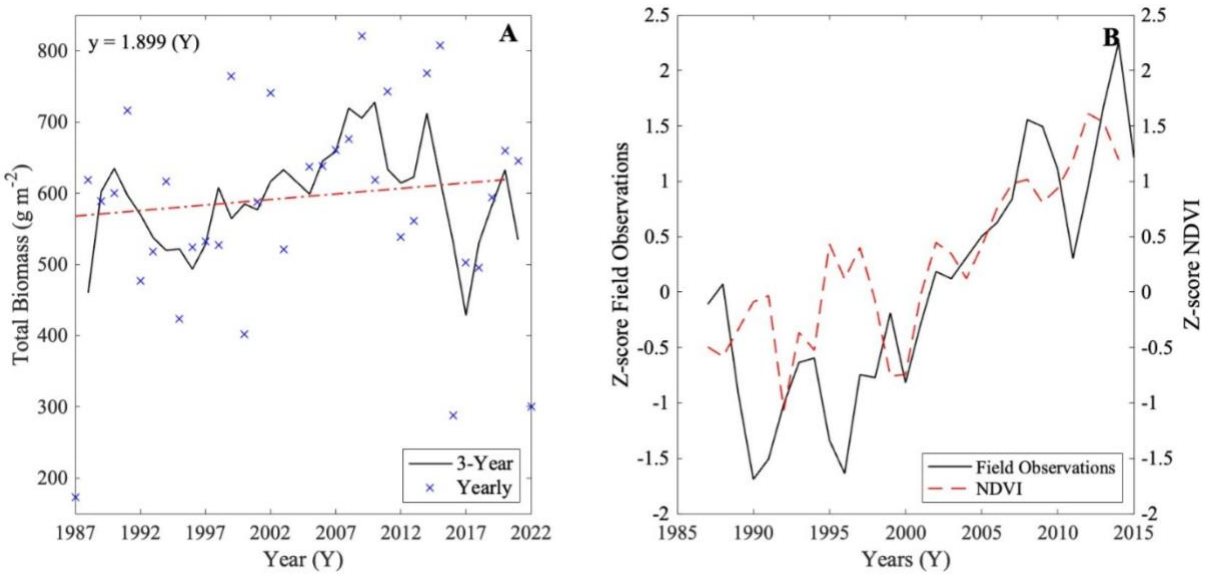

Figure 8 The (A) changes in average maximum total biomass from field observed data at the CSE site and the (B) z-score of the field observations and its corresponding NDVI values. In A the black line represents the 3-year moving window, the blue x's show the yearly average maxima and the red curve the overall trend over time. In B the black line shows the field observations and the red dashed line the NDVI.

For the CSE sites an overall increase in average maximum total biomass was found of 1.9 g m^{-2} $year^{-1}$ between 1985 and 2022 (Figure 8A). The biomass showed large inter-annual variation, ranging between ~ 200 g m^{-2} and ~ 800 g m^{-2}. Despite the overall positive trend three stronger dips in biomass occurred. These were between 1992 - 1996, 2010 – 2012 and the greatest between 2014 – 2017 where the total biomass dropped by ~ 300 g m^{-2}. These dips were often followed by rises in biomass in the following years.

The z-scores of the field observation at the CSE site and the NDVI showed a similar trend (Figure 8B). At the beginning of the study period a few differences are evident, namely in 1990 and between 1995 and 1997 where the field observations show a negative z-score, and that of NDVI was zero or positive. Both the field observations and NDVI show (mostly) negative z-scores until 2001, after which they continue to rise. This positive rise means a strong increase in biomass/fractional vegetation cover between 2001 and 2015 at the CSE sites across Senegal.

4.2. Relationship Between Maximum Fractional Foliage and Precipitation

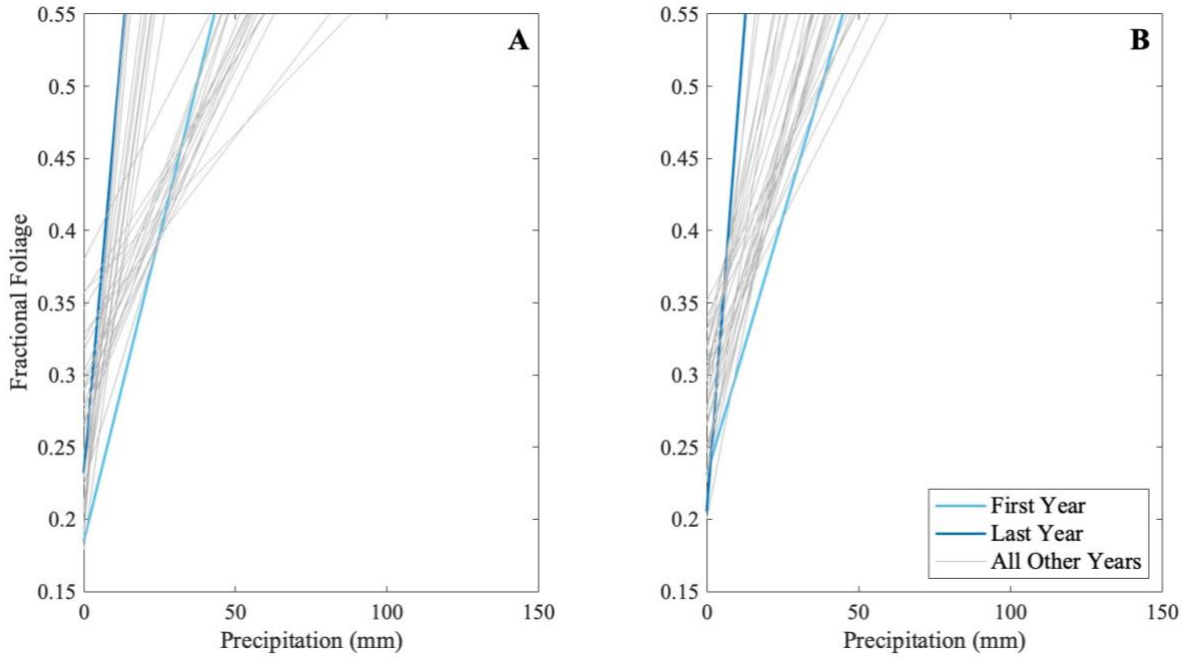

Figure 9 Linear section of curvilinear relationship between fractional foliage and precipitation in West Africa. Here A represents the initial technique of extracting the linear curve up to a fractional foliage of 0.55 and B the extraction of the linear section from the computed curvilinear relationship. In both plots the curves from 1984 and 1985 are excluded as they were identified as outliers.

The linear section of the curvilinear relationship between fractional foliage and precipitation using the linear plots (Figure 9A) and the curvilinear relationship (Figure 9B) in West Africa both showed an increasing slope between the first and the last year. A slight variation in y-intercept becomes evident in figure 9A, where a handful of plots had an intercept > 0.35 fractional foliage units whereas the rest range between 0.2 – 0.35. This is less evident in 9B, where only 1 plot had an intercept > 0.35.

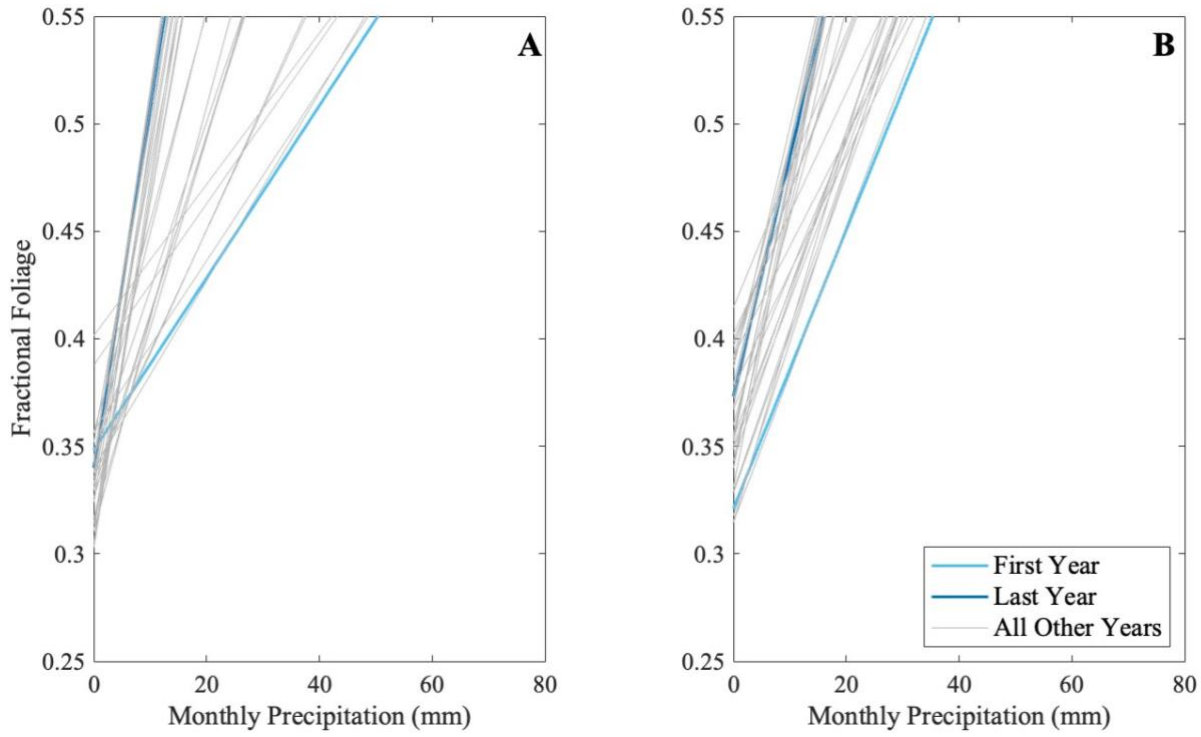

Figure 10 Linear section of curvilinear relationship between fractional foliage and precipitation in East Africa. Here A represents the initial technique of extracting the linear curve up to a fractional foliage of 0.55 and B the extraction of the linear section from the curvilinear relationship. Within A the years 1984, 1990 and 1995 are excluded after being identified as outliers, within B the year 1984 was excluded.

The linear sections of curvilinear relationship between precipitation and fractional foliage from the linear plots (Figure 10A) and from the curvilinear plots (Figure 10B) in East Africa both showed an increasing slope over time. This change in slope was greatest with the linear plots, where the last year showed a much steeper slope. With this changing slope the intercept remained quite stable around 0.35 for the linear plots. The curvilinear plots showed a greater intercept range, with most intercept being found between 0.3 – 0.4.

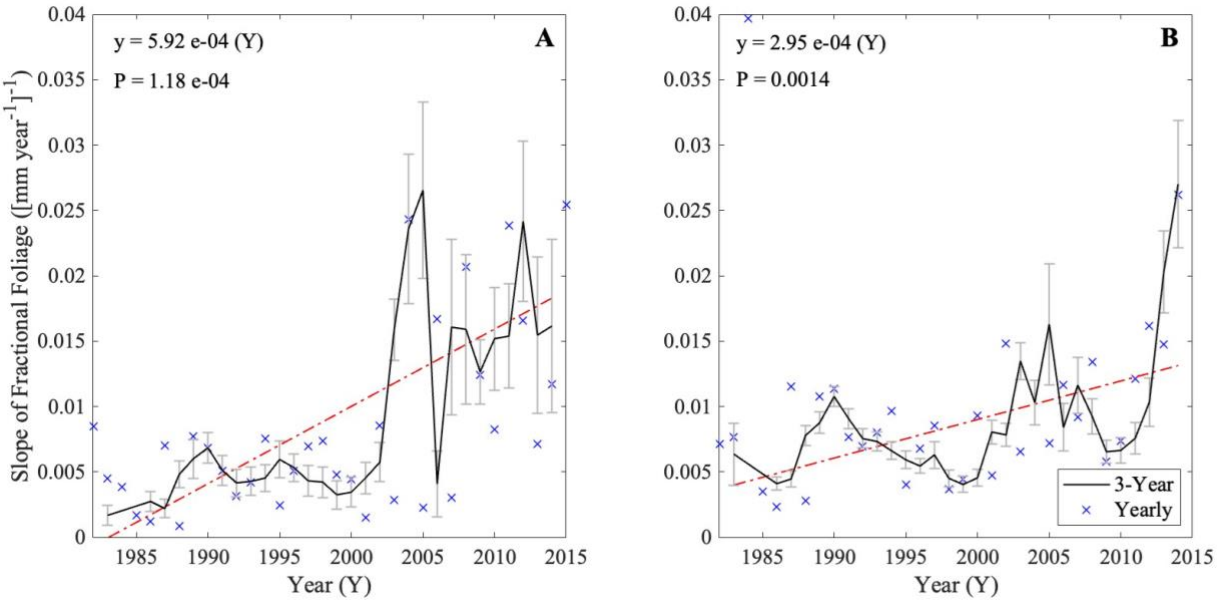

Figure 11 Time series of the change in the slope of fractional foliage to precipitation in West Africa. Here A represents the initial technique of extracting the linear curve up to a fractional foliage of 0.55 and B the extraction of the linear section from the curvilinear relationship. The black curve represents the three-year moving window, the blue x's show the yearly values, the red line represents the linear trend, as described by y, the error bars are the standard error and P shows the statistical significance using the Kendall- Tau test. In both figures the slopes from 1984 and 1985 are excluded after being identified as outliers.

Looking at the slope changes over time of the linear plots in Figure 9 it can be seen in Figure 11 that there was an overall statistically significant increase in fractional foliage of 5.92×10^{-4} and 2.95×10^{-4} [mm^{-1} $year^{-1}$]$^{-1}$ for the linear and curvilinear methods respectively (Figure 11). Even though both methods showed a similar overall trend, the linear fits showed steeper changes in slope, especially at the end of the study period (Figure 11A). This was seen in the steep rising slope around 2003 and the in the dip around 2006. The start of the study period on the other hand showed a more stable slope. The slope of the curvilinear plots on the other hand showed more gradual changes in slope (Figure 11B). Throughout the study period three clear dips can be identified, namely around 1986, 1999 and 2010. The last three years showed a steep and continuously rising slope.

The dips and peaks throughout the study period could be identified within both figures. With the exception of the peak in 2004, these dips and peaks could most clearly be identified with the slope changes on the curvilinear plots. The main differences were seen at the end of the study period, where the slope on the linear plots started to decrease again, while the slope of the curvilinear plots continued to increase.

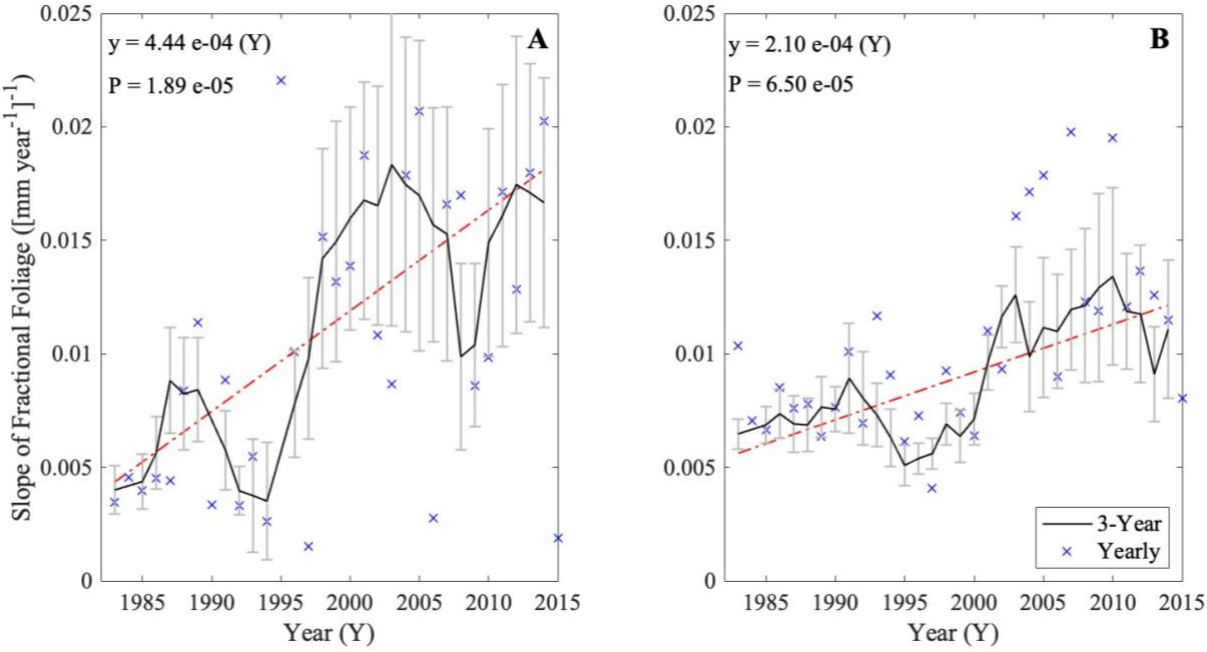

Figure 12 Time series of the changes in the slope of fractional foliage to precipitation in East Africa. Here A shows the slope of the linear plots between fractional foliage of 0.05 and 0.55 and B the slope of the linear section of the curvilinear relationship. The black curve represents the three-year moving window, the blue x's show the yearly values, the red line represents the linear trend, as described by y, the error bars are the standard error and P shows the statistical significance using the Kendall- Tau test. Within figure A the years 1984, 1990 and 1995 are excluded after being identified as outliers, within B the year 1984 was excluded.

The changing slopes over time from Figure 10, plotted in Figure 12, both showed a statistically significant increasing trend of 4.44 $x10^{-4}$ and 2.10 $x10^{-4}$ [mm $year^{-1}]^{-1}$ for the linear and curvilinear methods respectively (Figure 12), with the strongest dip found in 1995. With the linear plots the graph could generally be divided in two sections, one of a lower slope, between 1983 and 1995, and that of a higher slope, between 1998 and 2014 (Figure 12A). These sections were separated by a sharp rise in slope from ~ 2.5 $x10^{-3}$ to ~ 1.4 $x10^{-2}$ over two years. Over the study period two stronger dips were found, namely in 1990 and in 2009. On the other hand, the curvilinear relationships showed a more gradual rising trend, with a falling slope between 1991 and 1995 and between 2004 (Figure 12B). Here the slope over the entire period ranged between ~ 5.0 $x10^{-3}$ and ~1.3 $x10^{-2}$, whereas that of the linear plots ranged between ~ 2.5 $x10^{-3}$ and ~ 1.8 $x10^{-2}$.

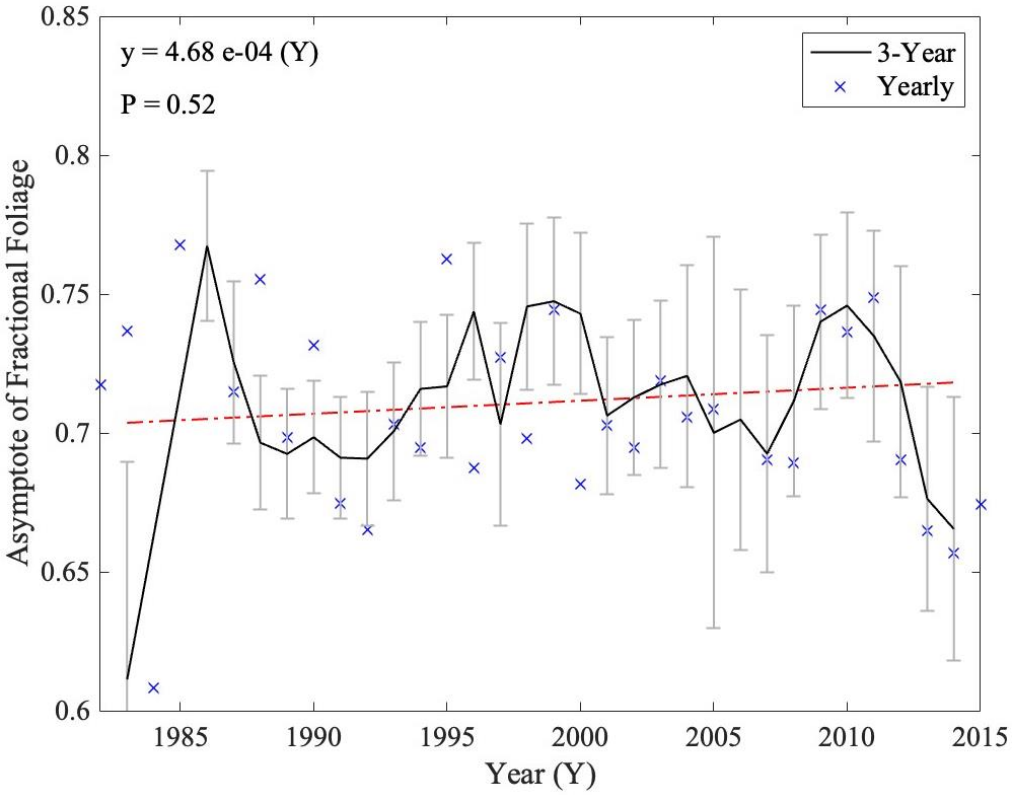

Figure 13 The asymptote of the curvilinear relationship between fractional foliage and precipitation plotted as the black curve. The red line represents the linear trend, described by y, the blue x's represent the yearly data, the error bars are the standard error and P shows the statistical significance using the Kendall- Tau test. The years 1984 and 1985 were excluded after being identified as outliers.

A statistically insignificant positive trend of the asymptote, of the relationship between fractional foliage and precipitation, in West Africa of 4.68 x 10^{-4} $year^{-1}$ was found (Figure 13). The data showed three dips: between 1988 and 1992, in 1997 and between 2000 and 2007. Despite the overall positive trend, the asymptote seemed to be decreasing the last few years of the study period.

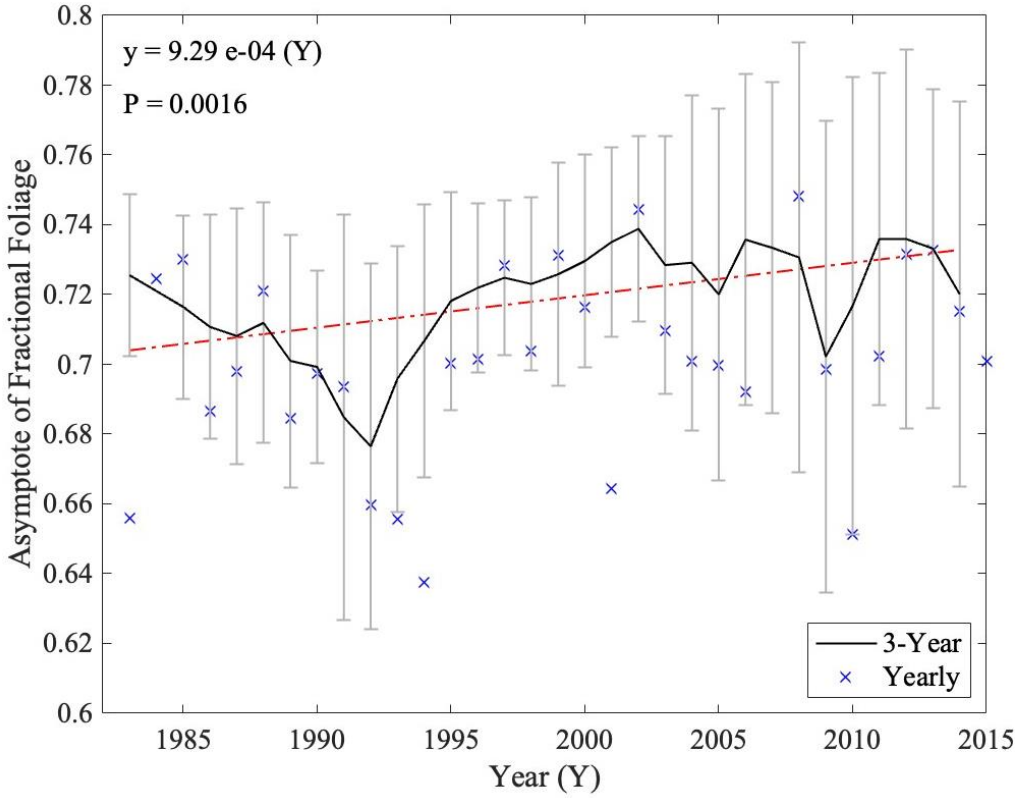

Figure 14 The asymptote of the curvilinear relationship between fractional foliage and precipitation plotted as the black curve. The red line represents the linear trend, described by y, the blue x's represent the yearly data, the error bars are the standard error and P shows the statistical significance using the Kendall- Tau test. The year 1984 was excluded after being identified as an outlier.

The asymptote of the curvilinear relationship between fractional foliage and precipitation in East Africa showed a statistically significant rise of 9.29 x 10^{-4} $year^{-1}$ (Figure 14). The curve showed a relatively stable trend, fluctuating between ~ 0.68 and ~ 0.74 fractional foliage units. Over the study period three dips were found, namely in, 1992, 2005 and 2009, of which the greatest in 1992, where the asymptote fell below 0.68.

5. Discussion

5.1. Changing Foliage Cover

Average foliage cover in the semi-arid and arid regions of West Africa showed a clear spatial gradient, with the highest cover found in the south of the study area, gradually decreasing when moving northwards. The gradient represents the movement from the Sahel in the south, with sparse vegetation, towards the Sahara, with little to no vegetation cover (Knauer et.al., 2014). Between 1982 and 2015 the greatest changes in fractional foliage were found within the region of higher foliage in the south. Here the changes spread around in a patchy pattern, not being isolated to a single area. Overall, an increase in average maximum foliage cover of 0.2 % per year was measured within this region. This is in accordance with other studies, who found a positive NDVI trend during this time (e.g., Dardel et.al., 2015; Fensholt et.al., 2012), however a different magnitude than Herrmann et.al. (2005), who found an up to 50 % increase in average NDVI between 1982 and 2003. Due to being a dynamic environment, this increase was not deemed meaningful, and strongly related to the return of normal rainfall conditions after an extended period of drought (Herrmann et.al., 2005).

Similar to the fractional foliage, the field observation biomass data from the CSE sites in Senegal showed a positive trend over time. This trend can mostly be explained by an increase in woody biomass, as it follows a similar trend, whereas the herbaceous cover decreased during the study period (Appendix 1). This is supported by Ripley et.al., (2022), who found that within savannas eCO_2 promoted the growth of woody biomass over that of C_4 grasses. It is suggested that, when looking at the z-scores of these field observations in comparison to NDVI, a similar interannual variability can be found. Similar results are found by Tian et.al., (2016), who found the data to be consistent with satellite time series. Here the green biomass showed a significant relationship to NDVI over the study period. With this it is assumed that the changes in the biomass data of the CSE site are comparable to the NDVI, and thus the fractional foliage used within the study. On the other hand, the Dahra site within Senegal showed a decrease in dry matter over time. The site showed a sharp decrease in dry matter between 2010 – 2012. In 2010 the dominating species was found to have changed, including the species Zornia which differs from grasses in botanical and ecological terms (Mbow et.al., 2013). This species covers the surface with thick leaves while remaining short and close to the ground resulting in a low biomass (Tagesson et.al., 2015). It was furthermore suggested that the inter-annual variability could be driven by non-environmental variables such as grazing, disturbance and herbivory (Tagesson et.al., 2016). Seeing as the Dahra site consists of solely one location in Senegal, in comparison to the 24 locations for the CSE study, it is suggested that the CSE site is more representative than the Dahra site. Looking at the z-scores of NDVI and the Dahra site they showed a similar interannual variability. These results were however limited to only 7 years in which there was an overlap of field observation and NDVI data. Despite a similar trend being found with the field observations and NDVI within this thesis, Dardel et.al., (2015) highlights

uncertainties when comparing biomass to NDVI data. Such uncertainties include the soil effects on NDVI, grazing pressures, land use and farming or floristic composition, all of which could result in a difference in the remotely sensed data in comparison to field observations.

The semi-arid and arid regions are spread across East Africa. Within these regions the average fractional foliage during the study period ranged between 0 and ~ 0.8 fractional foliage units. Throughout the study period the greatest changes in fractional foliage could be found in those regions with the highest average fractional foliage. Overall, a rise in average maximum foliage was measured of 0.11 % per year between 1982 and 2015. Zhao et.al. (2018), linked the rising trend to El Niño-Southern Oscillation and Interdecadal Pacific Oscillation events. Despite this, the area also showed regions with a decrease in fractional foliage. Hoscilo et.al. (2015) linked the decreasing NDVI to non-climatic land degradation in the Horn of Africa, where there was a strong rise in population. This led to a replacement of herbaceous and shrub vegetation cover to bare ground.

5.2. Effect of CO_2 Fertilisation

Following the rising trend in slope between precipitation and fractional foliage in West Africa, the hypothesis, based on the G-Range model, can be rejected. Within this model a strong decrease in biomass was predicted in West Africa by 2050 under RCP8.5 (Boone et.al., 2018). These changes were modelled to be driven by eCO_2 conditions in the G-range model. Earth observation data from 1982 to 2015 instead showed a continuous rise in fractional foliage driven by CO_2 fertilisation, with the results of the curvilinear plots showing an even steeper rise in slope in the last three studied years in West Africa (Figure 11B). The G-Range model further predicted a minimal change in biomass in East Africa (Boone et.al.2018), a change which was found within this study. When comparing the two regions, West Africa showed a greater change in slope, in the relationship between precipitation and fractional foliage, than East Africa, despite the slope being positive rather than negative in West Africa, this difference in magnitude was predicted by the model. A similar result was found by Ukkola et.al. (2016), here the maximum NDVI for a given precipitation level was measured to increase over time in water-limited areas of Australia. These results implied greater production under the same precipitation levels, which is consistent with CO_2 fertilisation. An overall positive influence of CO_2 fertilisation on fractional foliage for all arid and semi-arid regions globally was further found by Donohue et.al. (2013). These results imply that CO_2 fertilisation still has a positive influence in arid and semi-arid regions.

Strong inter-annual variability could be found within the rising slope in both East and West Africa. A possible explanation would be the variability in atmospheric CO_2 concentrations. It was proposed that the variability in CO_2 net ecosystem exchange was the driver of the inter-annual variability in the growth rates of atmospheric CO_2 concentrations (Marcolla et.al., 2017). The inter-annual variability found in West Africa was further suggested

to be attributed to greater inter-annual variability in growing season length, temperature and/or precipitation in future climate (Ahmed et.al., 2015).

In addition to a rising slope between precipitation and fractional foliage, a significant and insignificant rise in the asymptote of the curvilinear relationship was found in East and West Africa respectively. This asymptote represents the point at which the vegetation is no longer water limited (Ukkola et.al., 2016). When studying semi-arid regions in Australia Ukkola et.al. (2016) however found a reduction in this asymptote, relating it to the relaxation of vegetation to water limitations due to the increase in WUE from CO_2 fertilisation. The insignificant rising asymptote in West Africa may suggest that the NDVI was no longer water-limited and was not dependent on CO_2 fertilisation anymore. This brings the question if factors other than CO_2 fertilisation brought the rising asymptote in East Africa.

Following the plotted influence of CO_2 on fractional foliage the positive trend is expected to continue in the future for both East and West Africa. Ghannoum et.al. (2000) found that the growth stimulation of C4 plants in response to a doubling of CO_2 was lower than that of C3 plants, but that the magnitude of growth in C4 plants increased under elevated CO_2 with decreasing soil water availability. Under these conditions the plant overcomes the intercellular CO_2 partial pressure limitation of the CO_2 assimilation rate, imposed by low stomatal conductance, leading to higher CO_2 assimilation under elevated CO_2. With this, active photosynthesis and growth is extended in droughts under elevated CO_2, if other growth factors remain favourable. In doing so the plant is able to grow for longer during a drought. It was suggested that a C4 plant would lower leaf stomatal conductance and transpiration rates and increase leaf WUE to reduce the adverse effects of a drought under eCO_2, allowing photosynthesis to continue longer under the stressful and water-limited conditions (Vu & Allen, 2009; Sonmez et.al., 2020; Bendall et.al., 2022; Ripley et.al., 2022). Furthermore, the enhanced leaf WUE was found to increase soil water saving, reducing the water constraint of plant growth (Reich et.al., 2014). By limiting transpiration water loss during a drought, leaf mass per unit area was found to also increase due to water limitation (Bendall et.al., 2022). The strategy to increase leaf mass per unit area is applied by the plant to reduces wilting and conserves resources. This becomes increasingly important in the future, as East and West Africa are predicted to become more prone to droughts (Sylla et.al., 2016; Dosio et.la., 2021; Liu et.al., 2018; Nguvava et.al., 2019).

Despite that the CO_2 fertilisation effect could have a possible positive influence on growth during drought conditions in semi-arid areas, it could also induce Nitrogen (N) limitations in the plant by reducing the mineralization of soil organic matter (Srivastava et.al., 2012). This N limitation may limit the effect of CO_2 fertilisation as it is suggested to be dependent on the levels of other resources (Reich et.al., 2014; Kou-Giesbrecht & Arora, 2022). Keane et.al. (2020) however found that in the short-term soil C cycle enzymes investment reduced, as Phosphorus (P) cycle enzymes increased under eCO_2. It is suggested that the eCO_2 would reduce the need to invest in C cycling enzymes allowing for the investment in P cycle

enzymes. The microbes would be able to use the additional C in an attempt to secure more P, a more limited nutrient. Through this, eCO_2 conditions may alleviate the plants' possible P limitation. On the other hand, the increased microbial and plant biomass stocks, as a response of eCO_2, may increase the nutrients immobilized, resulting in N limitation in infertile ecosystems (Dieleman et.al., 2012). This would suggest an increasingly closed N cycle, leading to a gradual depletion in N. With this, nutrients are expected to constrain growth on the long scale. Looking at the C:N ratio, Ripley et.al. (2022) found no change in relation to eCO_2, as both N-fixation and C assimilation were both stimulated. This difference in short- and long-term reaction to nutrient availability may explain the difference in results within past earth observation data and the future modelled response of vegetation to CO_2 fertilisation within the G-range model. If the long-term negative implications on nutrients through eCO_2 becomes evident a reduction in biomass could be the result.

Unlike CO_2 fertilisation, rising temperatures increase the rate of N mineralization by the plants (Kirschbaum, 1999). Soil organic matter decomposition is driven by the elevated temperatures, releasing plant available N (Kou-Giesbrecht & Arora, 2022). Within an environment with rising temperatures, this could counterbalance the negative influence on nutrient availability by CO_2 fertilisation. Yet by increasing the evaporative demand of the plant and reducing WUE, plants are negatively influenced by rising temperatures in water-limited environments. However, Hatfield & Dold (2019) state that the direct relationship between climatic parameters, such as temperature, and WUE are not detectable and are less obvious. This is due to the lack of a temperature response to growth for a given species. It is suggested that the combined effect of eCO_2 concentrations and rising temperatures may be species-specific, and that the combined effect on photosynthesis would reflect both genetic and environmental factors (Lewis et.al., 2015). Rising temperatures were found to affect stomatal conductance rather than the photosynthesis, thus having less of an influence on plant growth. With this it is suggested that the changes in growth measured within this study can be related to CO_2 fertilisation, rather than the rising temperatures.

5.3. Limitations and Future Studies

Within semi-arid and arid ecosystems soil moisture is an important water resource for the plants (Na et.al., 2021). A time-lagged correlation has been shown between NDVI and soil moisture (Na et.al., 2021; Ahmed et.al., 2017). NDVI was found to increase with increasing soil moisture (Zhang et.al., 2018b). The optimal correlation for this response becomes evident after a 1-to-2-month lag (Ahmed et.al., 2017). This is further emphasized by Ibrahim et.al. (2015) who found a linear relationship between NDVI and the precipitation of three months prior in the Sahel. Within this study however the only water resource considered was precipitation. It is suggested that within future studies this time-lag of soil moisture is taken into account. In doing so, another aspect influencing NDVI and plant growth is considered, and the effect of CO_2 fertilisation can be better understood.

Another source of error is the selection of maximum monthly NDVI rather than average monthly NDVI. It can be questioned if selecting maximum values is representative of the month, especially during the wet season where large differences in NDVI can be found within one month (Zhang et.al., 2018a). The selection of the maximum may have caused an upwards shift in the 95th percentile values later used for analysis. However, in selecting the maximum values the possibility of errors from clouds and aerosols was reduced (Vickers et.al., 2016).

Furthermore, outliers were identified using the residuals of each plot. In doing so 1 – 3 years of data were removed in the analysis of the trend over time. One example of such as outlier was from West Africa in 1985 (Appendix 2). Here it can be seen that the asymptote of the curvilinear relationship reaches higher than a fractional foliage of 1. Seeing as this year did not show a curvilinear relationship, no reasonable asymptote was reached. From figures 9 and 10 it can be questioned if more plots should however have been identified, especially when looking at the y-intercepts. For both East and West Africa certain plots remain to show an intercept different to the majority. It can thus be questioned if these plots would be reasonable to compare to the others.

When analysing the slope, the effect of CO_2 fertilisation is not the only possible explanation of the changes. Donohue et.al. (2013) found that a rise in slope could be explained by an increase in drought-onset severity. An increase in drought severity over time could then possibly explain the rising slope. Within this thesis this was however not taken into account, thus, to better understand the trends found it is suggested to further analyse drought-onset severity. By having multiple factors that could influence NDVI, it is suggested that a 3-year moving window may not be sufficient to reduce this variability within the data. It is proposed to enlarge the window size to further reduce the inter-annual variability.

Two different methods were used within this thesis to analyse the influence of CO_2 fertilisation on fractional foliage in East and West Africa. In general, the two methods showed a similar trend, with strong changes being identified in both. One noticeable difference can be found within the slope changes of West Africa, where a sharp rise and dip are found in 2003 and 2006 respectively within the linear plots (Figure 11A), changes which are not as evident from the curvilinear plots (Figure 11B). No explanation could be found for these strong changes within previous papers; thus, it is assumed to be the result of the methodology. Looking at the error bars of the two methods (Figure 11 & Figure 12) it can be noticed that those for the linear plots are larger than those of the curvilinear plots, especially for East Africa. This could possibly be because the curvilinear relationship was based on 54 data points, whereas the linear curves were formed from 4 – 20 plots, depending on the year. Minimizing the data used to formulate the curve increases its uncertainty. The variation in data points used is the result of, the amount of precipitation required to reach the limit of 0.55 fractional foliage units. In some years this occurred within the 4th precipitation bin, and in others only within the 20th. For these reasons it is suggested to use the curvilinear method within future research rather than the linear method.

5.4. Future Implications

By absorbing nearly half of anthropogenic CO_2 emissions, terrestrial ecosystems provide a service to society by limiting climate warming (Smith et.al., 2020; Jiang et.al., 2020). This service is dependent on the ecosystems' CO_2 fertilisation response. Yet the eCO_2 concentrations will likely place further pressure on water resources in the semi-arid regions of East and West Africa, regions which will become more prone to droughts in the future (Ukkola et.la., 2016). However, Lewis et.al. (2015) found a larger response of eCO_2 from pre-industrial to ambient concentrations compared to the response towards future predicted concentrations. The long-term exposure to CO_2 would reduce its influence on photosynthesis. With this, the pressure on water resources would be limited, and the predictions by Boone et.al. (2018) for West Africa could become apparent.

6. Conclusion

This thesis found that the semi-arid and arid regions in East and West Africa both showed a rise in fractional foliage cover during the study period, on average showing the greatest change in the regions with the highest foliage cover. Studying past Earth observations data showed that these changes could be linked to a positive influence of CO_2 fertilisation. This positive trend in West Africa resulted in a rejection of the hypothesis that Earth observation data from 1982 - 2015 would show a reduction in the response of maximum foliage cover to precipitation, assumed to be a proxy to CO_2 fertilisation effect. The rising slope in the relationship between fractional foliage and precipitation implied greater production under fixed precipitation levels, which is consistent with assumptions of this slope to be a proxy of CO_2 fertilisation. Additionally, both West and East Africa showed a rising trend in the asymptote of the relationship between precipitation and fractional foliage. This trend in West Africa was however found to be insignificant, suggesting that the NDVI at the point of asymptote was no longer water-limited, and thus not dependent on CO_2 fertilisation anymore. The rising trend in East Africa on the other hand was significant, implying the effect of other influences on vegetation growth than CO_2 fertilisation.

7. References

Ahmed, M., Else, B., Eklundh, L., Ardö, J., & Seaquist, J. (2017). Dynamic response of NDVI to soil moisture variations during different hydrological regimes in the Sahel region. *International Journal of Remote Sensing*, *38*(19), 5408-5429.

Ahmed, K. F., Wang, G., Yu, M., Koo, J., & You, L. (2015). Potential impact of climate change on cereal crop yield in West Africa. *Climatic change*, *133*, 321-334.

Anyamba, A., & Tucker, C. J. (2005). Analysis of Sahelian vegetation dynamics using NOAA-AVHRR NDVI data from 1981–2003. *Journal of arid environments*, *63*(3), 596-614

Assmann, J. J., Kerby, J. T., Cunliffe, A. M., & Myers-Smith, I. H. (2018). Vegetation monitoring using multispectral sensors—Best practices and lessons learned from high latitudes. *Journal of Unmanned Vehicle Systems*, *7*(1), 54-75.

Ayugi, B. O., & Tan, G. (2019). Recent trends of surface air temperatures over Kenya from 1971 to 2010. *Meteorology and Atmospheric Physics*, *131*, 1401-1413.

Beck, H. E., Zimmermann, N. E., McVicar, T. R., Vergopolan, N., Berg, A., & Wood, E. F. (2018). Present and future Köppen-Geiger climate classification maps at 1-km resolution. *Scientific data*, *5*(1), 1-12.

Beck, P. S., Atzberger, C., Høgda, K. A., Johansen, B., & Skidmore, A. K. (2006). Improved monitoring of vegetation dynamics at very high latitudes: A new method using MODIS NDVI. *Remote sensing of Environment*, *100*(3), 321-334.

Bellouin, N., Quaas, J., Gryspeerdt, E., Kinne, S., Stier, P., Watson-Parris, D., ... & Stevens, B. (2020). Bounding global aerosol radiative forcing of climate change. *Reviews of Geophysics*, *58*(1), e2019RG000660.

Bendall, E. R., Bedward, M., Boer, M., Clarke, H., Collins, L., Leigh, A., & Bradstock, R. A. (2022). Growth enhancements of elevated atmospheric [CO2] are reduced under drought-like conditions in temperate eucalypts. *Functional Ecology*, *36*(7), 1542-1558.

Boone, R. B., Conant, R. T., Sircely, J., Thornton, P. K., & Herrero, M. (2018). Climate change impacts on selected global rangeland ecosystem services. *Global change biology*, *24*(3), 1382-1393.

Booth, B. B., Dunstone, N. J., Halloran, P. R., Andrews, T., & Bellouin, N. (2012). Aerosols implicated as a prime driver of twentieth-century North Atlantic climate variability. *Nature*, *484*(7393), 228-232.

Boretti, A., & Florentine, S. (2019). Atmospheric CO2 concentration and other limiting factors in the growth of C3 and C4 plants. *Plants*, *8*(4), 92.

Camberlin, P. (2018). Climate of eastern Africa. In *Oxford research encyclopedia of climate science*.

Chuvieco, E. (2016). *Fundamentals of Satellite Remote Sensing: An Environmental Approach, second edition*. CRC Press.

Copernicus. (2022). *ERA5-Land monthly averaged data from 1950 to present*. Copernicus Climate Data Store . Retrieved January 16, 2023, from https://cds.climate.copernicus.eu/cdsapp#!/dataset/reanalysis-era5-land-monthly-means?tab=overview

Cronin, T. W. (2014). On the choice of average solar zenith angle. *Journal of the Atmospheric Sciences*, *71*(8), 2994-3003.

Dardel, C., Kergoat, L., Hiernaux, P., Mougin, E., Grippa, M., & Tucker, C. J. (2014). Re-greening Sahel: 30 years of remote sensing data and field observations (Mali, Niger). *Remote Sensing of Environment*, *140*, 350-364.

de Jong, R., Verbesselt, J., Schaepman, M. E., & De Bruin, S. (2012). Trend changes in global greening and browning: contribution of short-term trends to longer-term change. *Global Change Biology*, *18*(2), 642-655.

Dieleman, W. I., Vicca, S., Dijkstra, F. A., Hagedorn, F., Hovenden, M. J., Larsen, K. S., ... & Janssens, I. A. (2012). Simple additive effects are rare: a quantitative review of plant biomass and soil process responses to combined manipulations of CO2 and temperature. *Global change biology*, *18*(9), 2681-2693.

Donohue, R. J., Roderick, M. L., McVicar, T. R., & Farquhar, G. D. (2013). Impact of CO2 fertilization on maximum foliage cover across the globe's warm, arid environments. *Geophysical Research Letters*, *40*(12), 3031-3035.

Dosio, A., Jury, M. W., Almazroui, M., Ashfaq, M., Diallo, I., Engelbrecht, F. A., ... & Tamoffo, A. T. (2021). Projected future daily characteristics of African precipitation based on global (CMIP5, CMIP6) and regional (CORDEX, CORDEX-CORE) climate models. *Climate Dynamics*, *57*(11-12), 3135-3158.

Ekwurzel, B., Boneham, J., Dalton, M. W., Heede, R., Mera, R. J., Allen, M. R., & Frumhoff, P. C. (2017). The rise in global atmospheric CO2, surface temperature, and sea level from emissions traced to major carbon producers. *Climatic Change*, *144*(4), 579-590.

Fayech, D., & Tarhouni, J. (2021). Climate variability and its effect on normalized difference vegetation index (NDVI) using remote sensing in semi-arid area. *Modeling Earth Systems and Environment*, *7*, 1667-1682.

Fensholt, R., Langanke, T., Rasmussen, K., Reenberg, A., Prince, S. D., Tucker, C., ... & Wessels, K. (2012). Greenness in semi-arid areas across the globe 1981–2007—an Earth Observing Satellite based analysis of trends and drivers. *Remote sensing of environment*, *121*, 144-158.

Fraser, R. S., & Kaufman, Y. J. (1985). The relative importance of aerosol scattering and absorption in remote sensing. *IEEE transactions on geoscience and remote sensing*, (5), 625-633.

Funk, C., Davenport, F., Harrison, L., Magadzire, T., Galu, G., Artan, G. A., ... & Nsadisa, F. D. (2018). 18. Anthropogenic enhancement of moderate-to-strong El Niño events likely contributed to drought and poor harvests in southern Africa during 2016. *Bull. Am. Meteorol. Soc*, *99*, S91-S96.

Ghannoum, O., Caemmerer, S. V., Ziska, L. H., & Conroy, J. P. (2000). The growth response of C4 plants to rising atmospheric CO2 partial pressure: a reassessment. *Plant, Cell & Environment*, *23*(9), 931-942.

Giannini, A., & Kaplan, A. (2019). The role of aerosols and greenhouse gases in Sahel drought and recovery. *Climatic Change*, *152*(3-4), 449-466.

Gifford, R. M. (2004). The CO2 Fertilising Effect: Does It Occur in the Real World?. *New Phytologist*, 221-225.

Gudoshava, M., Misiani, H. O., Segele, Z. T., Jain, S., Ouma, J. O., Otieno, G., ... & Atheru, Z. (2020). Projected effects of 1.5 C and 2 C global warming levels on the intra-seasonal rainfall characteristics over the Greater Horn of Africa. *Environmental Research Letters*, *15*(3), 034037.

Hatfield, J. L., & Dold, C. (2019). Water-use efficiency: advances and challenges in a changing climate. *Frontiers in plant science*, *10*, 103.

Helldén, U., & Tottrup, C. (2008). Regional desertification: A global synthesis. *Global and Planetary Change*, *64*(3-4), 169-176.

Herrmann, S. M., Anyamba, A., & Tucker, C. J. (2005). Recent trends in vegetation dynamics in the African Sahel and their relationship to climate. *Global Environmental Change*, *15*(4), 394-404.

Hickler, T., Eklundh, L., Seaquist, J. W., Smith, B., Ardö, J., Olsson, L., ... & Sjöström, M. (2005). Precipitation controls Sahel greening trend. *Geophysical Research Letters*, *32*(21).

Holden, P. B., Edwards, N. R., Gerten, D., & Schaphoff, S. (2013). A model-based constraint on CO 2 fertilisation. *Biogeosciences*, *10*(1), 339-355.

Horvath, H. (1993). Atmospheric light absorption—A review. *Atmospheric Environment. Part A. General Topics*, *27*(3), 293-317.

Hoscilo, A., Balzter, H., Bartholomé, E., Boschetti, M., Brivio, P. A., Brink, A., ... & Pekel, J. F. (2015). A conceptual model for assessing rainfall and vegetation trends in sub-Saharan Africa from satellite data. *International Journal of Climatology*, *35*(12), 3582-3592.

Huang, S., Tang, L., Hupy, J. P., Wang, Y., & Shao, G. (2021). A commentary review on the use of normalized difference vegetation index (NDVI) in the era of popular remote sensing. *Journal of Forestry Research*, *32*(1), 1-6.

Ibrahim, Y. Z., Balzter, H., Kaduk, J., & Tucker, C. J. (2015). Land degradation assessment using residual trend analysis of GIMMS NDVI3g, soil moisture and rainfall in Sub-Saharan West Africa from 1982 to 2012. *Remote Sensing*, *7*(5), 5471-5494.

Imran, H. A., Gianelle, D., Rocchini, D., Dalponte, M., Martín, M. P., Sakowska, K., ... & Vescovo, L. (2020). VIS-NIR, red-edge and NIR-shoulder based normalized vegetation indices response to co-varying leaf and Canopy structural traits in heterogeneous grasslands. *Remote Sensing*, *12*(14), 2254.

IPCC. (2022). *Climate change 2022: Impacts, adaptation and vulnerability*. IPCC . Retrieved October 15, 2022, from https://www.ipcc.ch/report/ar6/wg2/

Jiang, M., Medlyn, B. E., Drake, J. E., Duursma, R. A., Anderson, I. C., Barton, C. V., ... & Ellsworth, D. S. (2020). The fate of carbon in a mature forest under carbon dioxide enrichment. *Nature*, *580*(7802), 227-231.

Jong, S. M. D., Meer, F. D. V. D., & Clevers, J. G. (2004). Basics of remote sensing. *Remote sensing image analysis: Including the spatial domain*, 1-15.

Kalisa, W., Igbawua, T., Henchiri, M., Ali, S., Zhang, S., Bai, Y., & Zhang, J. (2019). Assessment of climate impact on vegetation dynamics over East Africa from 1982 to 2015. *Scientific reports*, *9*(1), 1-20.

Karthikeyan, L., Chawla, I., & Mishra, A. K. (2020). A review of remote sensing applications in agriculture for food security: Crop growth and yield, irrigation, and crop losses. *Journal of Hydrology*, *586*, 124905.

Keane, J. B., Hoosbeek, M. R., Taylor, C. R., Miglietta, F., Phoenix, G. K., & Hartley, I. P. (2020). Soil C, N and P cycling enzyme responses to nutrient limitation under elevated CO 2. *Biogeochemistry*, *151*, 221-235.

Kennedy, J., Dunn, R., McCarthy, M., Titchner, H., & Morice, C. (2017). Global and regional climate in 2016. *Weather*, *72*(8), 219-225.

Kirschbaum, M. U. (1999). Modelling forest growth and carbon storage in response to increasing CO2 and temperature. *Tellus B*, *51*(5), 871-888.

Knauer, K., Gessner, U., Dech, S., & Kuenzer, C. (2014). Remote sensing of vegetation dynamics in West Africa. *International Journal of Remote Sensing*, *35*(17), 6357-6396.

Kottek, M., Grieser, J., Beck, C., Rudolf, B., & Rubel, F. (2006). World map of the Köppen-Geiger climate classification updated.

Kou-Giesbrecht, S., & Arora, V. (2022). Compensatory Effects between CO2, Nitrogen Deposition, and Temperature in Terrestrial Biosphere Models without Nitrogen Compromise Projections of the Future Terrestrial Carbon Sink.

Krause, A. G., & Weis, E. (1991). Chlorophyll fluorescence and photosynthesis: the basics. *Annual review of plant biology*, *42*(1), 313-349.

Lewis, J. D., Phillips, N. G., Logan, B. A., Smith, R. A., Aranjuelo, I., Clarke, S., ... & Tissue, D. T. (2015). Rising temperature may negate the stimulatory effect of rising CO2 on growth and physiology of Wollemi pine (Wollemia nobilis). *Functional Plant Biology*, *42*(9), 836-850.

Liu, S., Ji, C., Wang, C., Chen, J., Jin, Y., Zou, Z., ... & Zou, J. (2018). Climatic role of terrestrial ecosystem under elevated CO 2: a bottom-up greenhouse gases budget. *Ecology Letters*, *21*(7), 1108-1118.

Manatsa, D., & Behera, S. K. (2013). On the epochal strengthening in the relationship between rainfall of East Africa and IOD. *Journal of Climate*, *26*(15), 5655-5673.

Marchant, R., Richer, S., Boles, O., Capitani, C., Courtney-Mustaphi, C. J., Lane, P., ... & Wright, D. (2018). Drivers and trajectories of land cover change in East Africa: Human and environmental interactions from 6000 years ago to present. *Earth-Science Reviews*, *178*, 322-378.

Marcolla, B., Rödenbeck, C., & Cescatti, A. (2017). Patterns and controls of inter-annual variability in the terrestrial carbon budget. *Biogeosciences*, *14*(16), 3815-3829.

Mbow, C., Fensholt, R., Rasmussen, K., & Diop, D. (2013). Can vegetation productivity be derived from greenness in a semi-arid environment? Evidence from ground-based measurements. *Journal of Arid Environments*, *97*, 56-65.

Na, L., Na, R., Bao, Y., & Zhang, J. (2021). Time-lagged correlation between soil moisture and intra-annual dynamics of vegetation on the Mongolian plateau. *Remote Sensing*, *13*(8), 1527.

Neinavaz, E., Schlerf, M., Darvishzadeh, R., Gerhards, M., & Skidmore, A. K. (2021). Thermal infrared remote sensing of vegetation: Current status and perspectives. *International Journal of Applied Earth Observation and Geoinformation*, *102*, 102415.

Nguvava, M., Abiodun, B. J., & Otieno, F. (2019). Projecting drought characteristics over East African basins at specific global warming levels. *Atmospheric Research*, *228*, 41-54.

Ni, Z. Z., Luo, K., Zhang, J. X., Feng, R., Zheng, H. X., Zhu, H. R., ... & Cen, K. F. (2018). Assessment of winter air pollution episodes using long-range transport modeling in Hangzhou, China, during World Internet Conference, 2015. *Environmental pollution*, *236*, 550-561.

Nicholson, S. E. (2017). Climate and climatic variability of rainfall over eastern Africa. *Reviews of Geophysics*, *55*(3), 590-635.

Nielsen, U. N., & Ball, B. A. (2015). Impacts of altered precipitation regimes on soil communities and biogeochemistry in arid and semi-arid ecosystems. *Global change biology*, *21*(4), 1407-1421.

Nikiema, P. M., Sylla, M. B., Ogunjobi, K., Kebe, I., Gibba, P., & Giorgi, F. (2017). Multi-model CMIP5 and CORDEX simulations of historical summer temperature and precipitation variabilities over West Africa. *International Journal of Climatology*, *37*(5), 2438-2450.

NOAA, U. S. D. of C. (2022). *Global Monitoring Laboratory - Carbon Cycle Greenhouse Gases*. GML. Retrieved January 19, 2023, from https://gml.noaa.gov/ccgg/mbl/data.php

Olsson, L., Eklundh, L., & Ardö, J. (2005). A recent greening of the Sahel—trends, patterns and potential causes. *Journal of Arid Environments*, *63*(3), 556-566.

openAfrica. (2020, April 21). *OpenAFRICA*. openAFRICA. Retrieved March 13, 2023, from https://open.africa/dataset/africa-shapefiles

Park, S., Kang, D., Yoo, C., Im, J., & Lee, M. I. (2020). Recent ENSO influence on East African drought during rainy seasons through the synergistic use of satellite and reanalysis data. *ISPRS Journal of Photogrammetry and Remote Sensing*, *162*, 17-26.

Peel, M. C., B. L. Finlayson, and T. A. McMahon (2007), Updated world map of the 300 Köppen-Geiger climate classification, Hydrology and Earth System Sciences, 11(5), 301 1633-1644

Pettorelli, N., Vik, J. O., Mysterud, A., Gaillard, J. M., Tucker, C. J., & Stenseth, N. C. (2005). Using the satellite-derived NDVI to assess ecological responses to environmental change. *Trends in ecology & evolution*, *20*(9), 503-510.

Piao, S., Wang, X., Park, T., Chen, C., Lian, X. U., He, Y., ... & Myneni, R. B. (2020). Characteristics, drivers and feedbacks of global greening. *Nature Reviews Earth & Environment*, *1*(1), 14-27.

Ranasinghe, R., Ruane, A. C., Vautard, R., Arnell, N., Coppola, E., Cruz, F. A., ... & Zaaboul, R. (2021). Climate change information for regional impact and for risk assessment.

Reich, P. B., Hobbie, S. E., & Lee, T. D. (2014). Plant growth enhancement by elevated CO2 eliminated by joint water and nitrogen limitation. *Nature Geoscience*, *7*(12), 920-924.

Ripley, B. S., Raubenheimer, S. L., Perumal, L., Anderson, M., Mostert, E., Kgope, B. S., ... & Simpson, K. J. (2022). CO2-fertilisation enhances resilience to browsing in the recruitment phase of an encroaching savanna tree. *Functional Ecology*, *36*(12), 3223-3233.

Rowell, D. P., Booth, B. B., Nicholson, S. E., & Good, P. (2015). Reconciling past and future rainfall trends over East Africa. *Journal of Climate*, *28*(24), 9768-9788.

Schwalm, C. R., Glendon, S., & Duffy, P. B. (2020). RCP8. 5 tracks cumulative CO2 emissions. *Proceedings of the National Academy of Sciences*, *117*(33), 19656-19657.

Shevela, D., & Bjorn, L. O. (2018). *Photosynthesis: solar energy for life*. World Scientific Publishing.

Smith, W. K., Fox, A. M., MacBean, N., Moore, D. J., & Parazoo, N. C. (2020). Constraining estimates of terrestrial carbon uptake: New opportunities using long-term satellite observations and data assimilation. *New Phytologist*, *225*(1), 105-112.

Sonmez, M. C., Ozgur, R., Uzilday, B., Turkan, I., & Ganie, S. A. (2022). Redox regulation in C3 and C4 plants during climate change and its implications on food security. *Food and Energy Security*, e387.

Srivastava, A. K., Gaiser, T., Paeth, H., & Ewert, F. (2012). The impact of climate change on Yam (Dioscorea alata) yield in the savanna zone of West Africa. *Agriculture, ecosystems & environment*, *153*, 57-64.

Stirbet, A., Lazár, D., Guo, Y., & Govindjee, G. (2020). Photosynthesis: basics, history and modelling. *Annals of Botany*, *126*(4), 511-537.

Sylla, M. B., Elguindi, N., Giorgi, F., & Wisser, D. (2016). Projected robust shift of climate zones over West Africa in response to anthropogenic climate change for the late 21st century. *Climatic Change*, *134*(1-2), 241-253.

Tagesson, T., Fensholt, R., Guiro, I., Rasmussen, M. O., Huber, S., Mbow, C., ... & Ardö, J. (2015). Ecosystem properties of semiarid savanna grassland in West Africa and its relationship with environmental variability. *Global change biology*, *21*(1), 250-264.

Tagesson, T., Ardö, J., Guiro, I., Cropley, F., Mbow, C., Horion, S., ... & Fensholt, R. (2016). Very high CO2 exchange fluxes at the peak of the rainy season in a West African grazed

semi-arid savanna ecosystem. *Geografisk Tidsskrift-Danish Journal of Geography*, *116*(2), 93-109.

Tao, S., Feng, H., Xu, Z., & Li, Q. (2012). Image degradation and recovery based on multiple scattering in remote sensing and bad weather condition. *Optics Express*, *20*(15), 16584-16595.

Tian, F., Brandt, M., Liu, Y. Y., Verger, A., Tagesson, T., Diouf, A. A., ... & Fensholt, R. (2016). Remote sensing of vegetation dynamics in drylands: Evaluating vegetation optical depth (VOD) using AVHRR NDVI and in situ green biomass data over West African Sahel. *Remote Sensing of Environment*, *177*, 265-276.

Tian, F., Fensholt, R., Verbesselt, J., Grogan, K., Horion, S., & Wang, Y. (2015). Evaluating temporal consistency of long-term global NDVI datasets for trend analysis. *Remote Sensing of Environment*, *163*, 326-340.

Ukkola, A. M., Prentice, I. C., Keenan, T. F., Van Dijk, A. I., Viney, N. R., Myneni, R. B., & Bi, J. (2016). Reduced streamflow in water-stressed climates consistent with CO2 effects on vegetation. *Nature Climate Change*, *6*(1), 75-78.

Vickers, H., Høgda, K. A., Solbø, S., Karlsen, S. R., Tømmervik, H., Aanes, R., & Hansen, B. B. (2016). Changes in greening in the high Arctic: insights from a 30 year AVHRR max NDVI dataset for Svalbard. *Environmental Research Letters*, *11*(10), 105004.

Wainwright, C. M., Marsham, J. H., Keane, R. J., Rowell, D. P., Finney, D. L., Black, E., & Allan, R. P. (2019). 'Eastern African Paradox'rainfall decline due to shorter not less intense Long Rains. *npj Climate and Atmospheric Science*, *2*(1), 34.

Wei, F., Wang, S., Fu, B., Pan, N., Feng, X., Zhao, W., & Wang, C. (2018). Vegetation dynamic trends and the main drivers detected using the ensemble empirical mode decomposition method in East Africa. *Land degradation & development*, *29*(8), 2542-2553.

Wiltshire, A. J., Kay, G., Gornall, J. L., & Betts, R. A. (2013). The impact of climate, CO2 and population on regional food and water resources in the 2050s. *Sustainability*, *5*(5), 2129-2151.

Wong, J. (2020). A greener planet. *New Scientist*, *246*(3282), 23.

World Bank. (2023). Data Catalog. Retrieved February 1, 2023, from https://datacatalog.worldbank.org/search/dataset/0042325

Xiao, J., & Moody, A. (2005). Geographical distribution of global greening trends and their climatic correlates: 1982–1998. *International Journal of Remote Sensing*, *26*(11), 2371-2390.

Yang, J., Gong, P., Fu, R., Zhang, M., Chen, J., Liang, S., ... & Dickinson, R. (2013). The role of satellite remote sensing in climate change studies. *Nature climate change*, *3*(10), 875-883.

Zhang, H., Chang, J., Zhang, L., Wang, Y., Li, Y., & Wang, X. (2018b). NDVI dynamic changes and their relationship with meteorological factors and soil moisture. *Environmental Earth Sciences*, *77*, 1-11.

Zhang, W., Brandt, M., Tong, X., Tian, Q., & Fensholt, R. (2018a). Impacts of the seasonal distribution of rainfall on vegetation productivity across the Sahel. *Biogeosciences*, *15*(1), 319-330.

Zhang, X., Zhang, Y., Ma, N., Kong, D., Tian, J., Shao, X., & Tang, Q. (2021). Greening-induced increase in evapotranspiration over Eurasia offset by CO2-induced vegetational stomatal closure. *Environmental Research Letters*, *16*(12), 124008.

Zhang, X., Zhang, Y., Tian, J., Ma, N., & Wang, Y. P. (2022). CO2 fertilization is spatially distinct from stomatal conductance reduction in controlling ecosystem water-use efficiency increase. *Environmental Research Letters*, *17*(5), 054048.

Zhao, L., Dai, A., & Dong, B. (2018). Changes in global vegetation activity and its driving factors during 1982–2013. *Agricultural and Forest Meteorology*, *249*, 198-209.

Zhu, Z., Piao, S., Myneni, R. B., Huang, M., Zeng, Z., Canadell, J. G., ... & Zeng, N. (2016). Greening of the Earth and its drivers. *Nature climate change*, *6*(8), 791-795.

8. Appendix

8.1. Appendix 1: Change in Herbaceous and Woody Biomass CSE

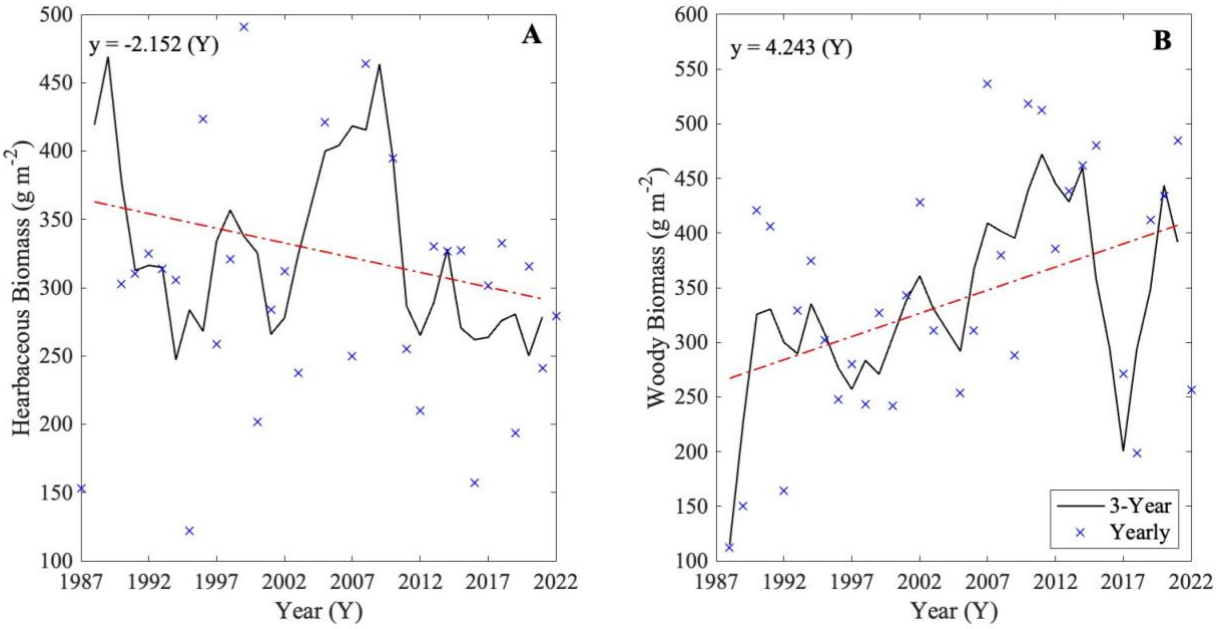

Figure 13 Changes in maximum herbaceous biomass (A) and woody biomass (B) at the CSE site. Here the black curve shows the 3-year moving window, the blue x's the yearly values, and the red line the overall relationship described by y.

8.2. Appendix 2: Outlier of Asymptote of Curvilinear Relationship in West Africa

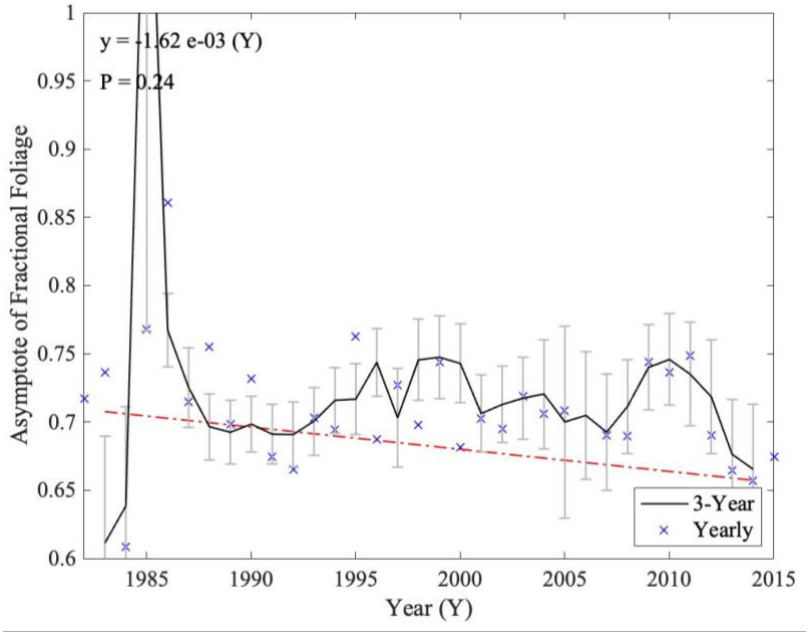

Figure 16 The extraction of the asymptote of the relationship between fractional foliage and precipitation plotted as the black curve. The red line represents the linear trend, described by y, the blue x's represent the yearly data, the error bars are the standard error and P is calculated using the Kendall- Tau test.

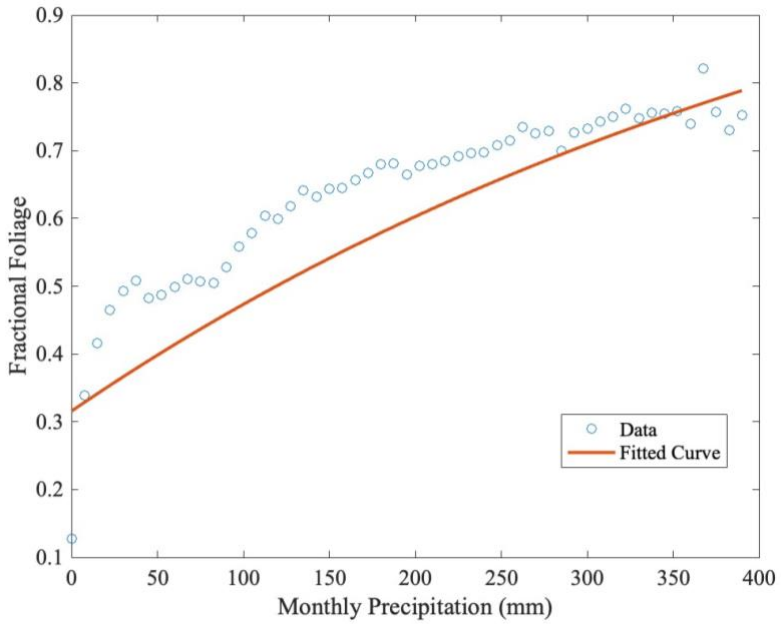

Figure 17 The computed curvilinear relationship of fractional foliage to monthly precipitation in 1985 from the 95th percentile values of each precipitation bin. Here the fitted data shows a more continuous gradient, without an asymptote being reached.